OSL Dating of a Coastal Swift Creek Occupation at Harrison Ring, Bay County, Florida

OSL Dating of a Coastal Swift Creek Occupation at Harrison Ring, Bay County, Florida

By KATHLEEN RODRIGUES, B.Sc.

A Thesis Submitted to the School of Graduate Studies in Partial Fulfillment of the Requirements for the Degree Master of Science

McMaster University MASTER OF SCIENCE (2015) Hamilton, Ontario (Earth Sciences)

TITLE: **OSL dating of a coastal Swift Creek occupation at Harrison Ring, Bay County, Florida**

AUTHOR: Rodrigues, K.S. (McMaster University)

SUPERVISOR: Professor W.J. Rink

NUMBER OF PAGES: 60

ABSTRACT

A total of 17 samples were collected for OSL dating from a Swift Creek archaeological site, known as Harrison Ring, which lies on the Tyndall Air force peninsula in northwest Florida. High-resolution vertical sampling conducted at 10 cm intervals from the surface was performed in order to determine the timing of occupation at the site, and to look for patterns in radiation dosimetry and post-depositional disturbance that can compromise OSL results. We find OSL ages determined using both 0.5 mm aliquots and single grains at the archaeological levels (approximately 1751 ± 339 years ago) to be consistent with the timing of early Swift Creek cultures on the Florida Gulf Coast. The ages we report are both consistent with radiocarbon dates taken at Harrison Ring, and those taken at other Swift Creek sites on the Gulf Coast. In general, we find OSL equivalent doses that show high overdispersion and skewness that we attribute to beta-microdosimetry and possible bioturbation in the profiles. We also present results from a test with a novel dosimetric technique employing Al_2O_3:C chips. By using Al_2O_3:C dosimeters, we find that large variability in beta dose rates exist in the sedimentary profile at Harrison Ring. By testing a combination of dosimetric techniques in a site with a well-constrained age, we find that the best agreement with independent age control exists when calculating ages using a beta dose rate from NAA/DNC and gamma dose rate from Al_2O_3:C dosimetry.

ACKNOWLEDGEMENTS

I would like to express my sincere thanks and gratitude to my supervisor, Dr. Jack Rink, for his constant encouragement and support over the course of this MSc research. The many valuable comments and suggestions I received from our discussions were critical to the development of this thesis.

Many thanks to others who contributed their knowledge and time, and were instrumental to the success of this research. Rebecca Saunders and Craig Dengel were important resources for understanding the site archaeology both in the field and outside the field. I also thank Dr. Regina DeWitt for her contribution of the Al_2O_3:C dosimeters as well as their analysis. Finally, I thank Dr. Amanda Keen-Zebert for giving me access to the single grain OSL facilities at the Desert Research Institute.

TABLE OF CONTENTS

LIST OF FIGURES

LIST OF TABLES

LIST OF EQUATIONS

LIST OF ABBREVIATIONS

a	Annum, years before present
ASL	Above sea level
D_E	Equivalent dose
DNC	Delayed Neutron Counting
FMM	Finite Mixture Model
MAM3	3-Parameter Minimum Age Model
NAA	Neutron Activation Analysis
OSL	Optically Stimulated Luminescence
REG	Regeneration
SAR	Single Aliquot Regenerative protocol
TAFB	Tyndall Air Force Base

CHAPTER 1: INTRODUCTION

1.1 Purpose of Study

The purpose of this study was to use OSL to examine an archaeological deposit using high-resolution vertical sampling. This high resolution OSL sampling was performed in order to determine the timing of occupation at the site, but also to look for patterns in radiation dosimetry and post-depositional disturbance that have the potential to compromise OSL results. Another major goal of this study was to test the application of in-situ Al_2O_3:C dosimeters by using them with OSL at a site with age control for the first time.. Al_2O_3:C dosimetry has only recently been adapted for use in sedimentary environments, and its utility has not yet been clearly tested in sedimentary environments with beta dose rate heterogeneity. By testing the use of both in-situ Al_2O_3:C dosimetry and dosimetry based on neutron activation analysis (NAA) of small sample volumes, we hope to gather insight on how to apply dosimetric techniques in low dose rate sedimentary environments affected by beta dose rate heterogenetiy.

1.2 Previous Studies

1.2.1 Archaeological background

The Swift Creek tradition has a time span dating from around A.D. 150 to A.D. 800 on the Florida Gulf Coast (Stephenson et al., 2002, Table 1). The Swift Creek culture is distinguished primarily by stratigraphic context and by the characteristic stylistic qualities seen in pottery forms made by this culture. The spatial extent of the Swift Creek culture is well defined, and covers northwest Florida, northeastern Florida, eastern Alabama, and Georgia as shown in Figure 1 (Williams and Elliott, 1998). The ceramic culture of the Swift Creek period is recognized by the intricate paddle-stamped ceramics that represent the oldest Complicated Stamped ceramics in the eastern United States. Among the most common site types in this cultural period are ring-shaped middens representing circular communities that surround a centralized plaza (Milanich, 1994).

Table 1 A generalized chronology of cultural periods in Florida (adapted from Milanich, 1994; Stephenson et al., 2002).

Period & Stage	Culture	Age	Age (years ago)
Early Woodland	Deptford	500 B.C. – 200 A.D.	2515 – 1815
Middle Woodland	Early Swift Creek	150 – 400 A.D.	1865 – 1615
	Late Swift Creek	400 – 800 A.D.	1615 - 1215
	Early Weeden Island	400 – 650 A.D.	1615 – 1365
Late Woodland	Late Weeden Island	650 – 1000 A.D.	1215 – 1015
Mississippian	Fort Walton	1000 – 1500 A.D.	1015 – 515

In northwest Florida, there are a total of ninety-nine Swift Creek sites that have been recorded in the state site files (Russo et al., 2009). Many of these sites have not been thoroughly surveyed and there are often gaps in survey coverage and intensity. Based on the findings that exist, there appear to be a trend with a high concentration of sites near the coast (87% of sites). Only twelve of the known sites are located interiorly, and are generally much smaller in area (Russo et al., 2009). This pattern has led many archaeologists to believe that Middle Woodland populations were concentrated in coastal areas, with interior lands typically left vacant and used for special-purpose, ephemeral activities. A second pattern observed for Swift Creek sites is related to their spatial configuration. Three main types of midden configuration exist among the identified Swift Creek sites: ring middens (circular, rectangular or horseshoe shaped), linear middens, and small midden dumps. Ring middens are typically large (approximately 100 m in diameter), shell-rich rings with heights of over 1 m, and have an interior sterile central plaza (Milanich, 1994). Between coastal Panama City and Pensacola, eight site clusters have been identified. In four of these, a ring midden is the main settlement, two of which have at least one associated burial mound. These ring middens were abandoned after Swift Creek occupation, and nearby areas were later occupied during the Late Swift Creek and Weeden Island periods (Milanich, 1994).

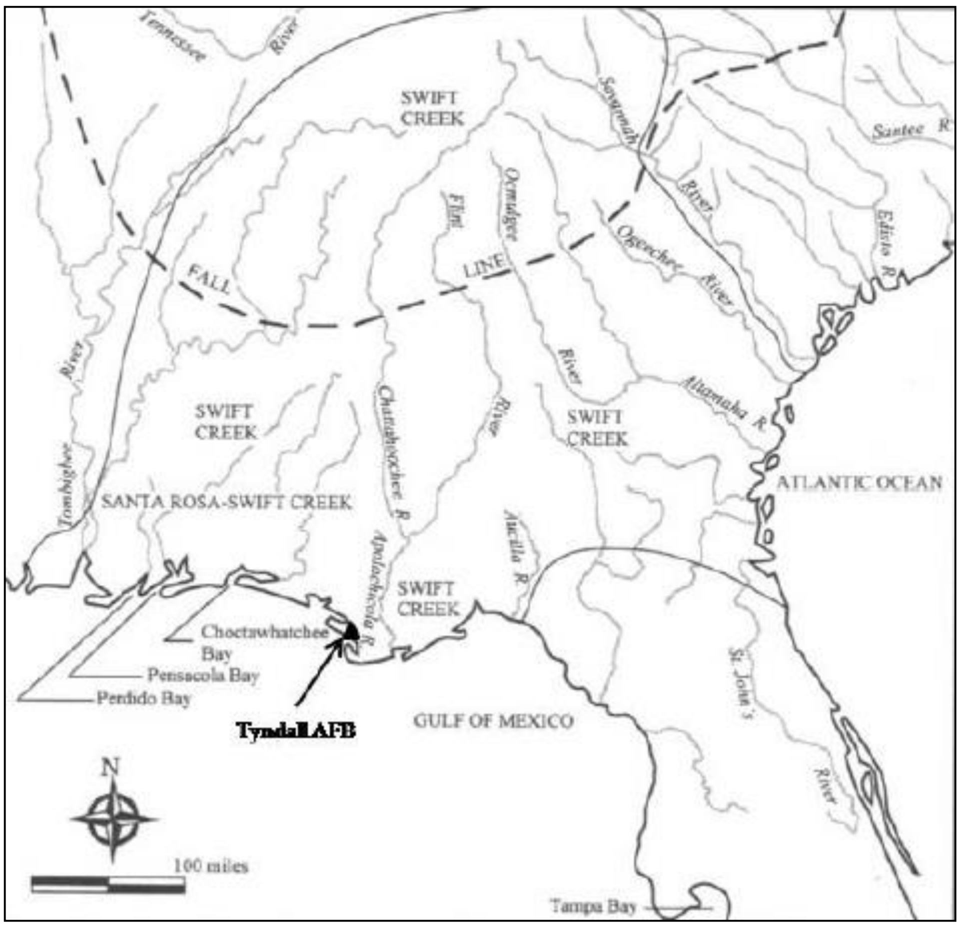

Figure 1 A map showing the geographical extent of the Swift Creek culture (Adapted from Russo et al., 2009; Williams and Elliott, 1998).

Swift creek ceramics are characterized by their intricate paddle-stamped designs. The stamps are typically curvilinear designs, with some incorporating linear motifs and features. A range of unique ceramic design attributes including lip treatments make Swift Creek ceramics well-suited to seriation (Milanich, 1994). These unique qualities have allowed archaeologists to make hypotheses about social interaction and the movement of either the ceramic vessels or the wooden paddles used in their manufacture (eg. Ashley and Wallis, 2006; Kirkland and Swight, 2003). The Swift creek tool kit includes stemmed projectile points, bifacial knives, spokeshaves, flake scrapers, abraders (limestone, sandstone and chert), and pitted anvil stones (Milanich, 1994).

Swift Creek religious and ceremonial practices have been defined by Sears as the Green Point-Hopewellian complex (Sears, 1962). The Hopewellian interaction sphere was one that involved long-distance trade networks with coexistent Woodland cultures in the eastern United States. The Swift Creek peoples interacted with other surrounding cultures through exchanges of exotic items, such as copper, greenstone, mica, conch shells and ceramics (Bense, 1989; Milanich, 1994). Many of the cultures that participated in the Hopewellian interaction sphere, like the Swift Creek, show evidence for a socio-political hierarchy. Separate sociological classes have become apparent in the archaeological record, with sacred paraphernalia being buried alongside high-status individuals in burial mounds (Milanich, 1994).

1.2.2 Archaeological investigations at the Hare Hammock complex

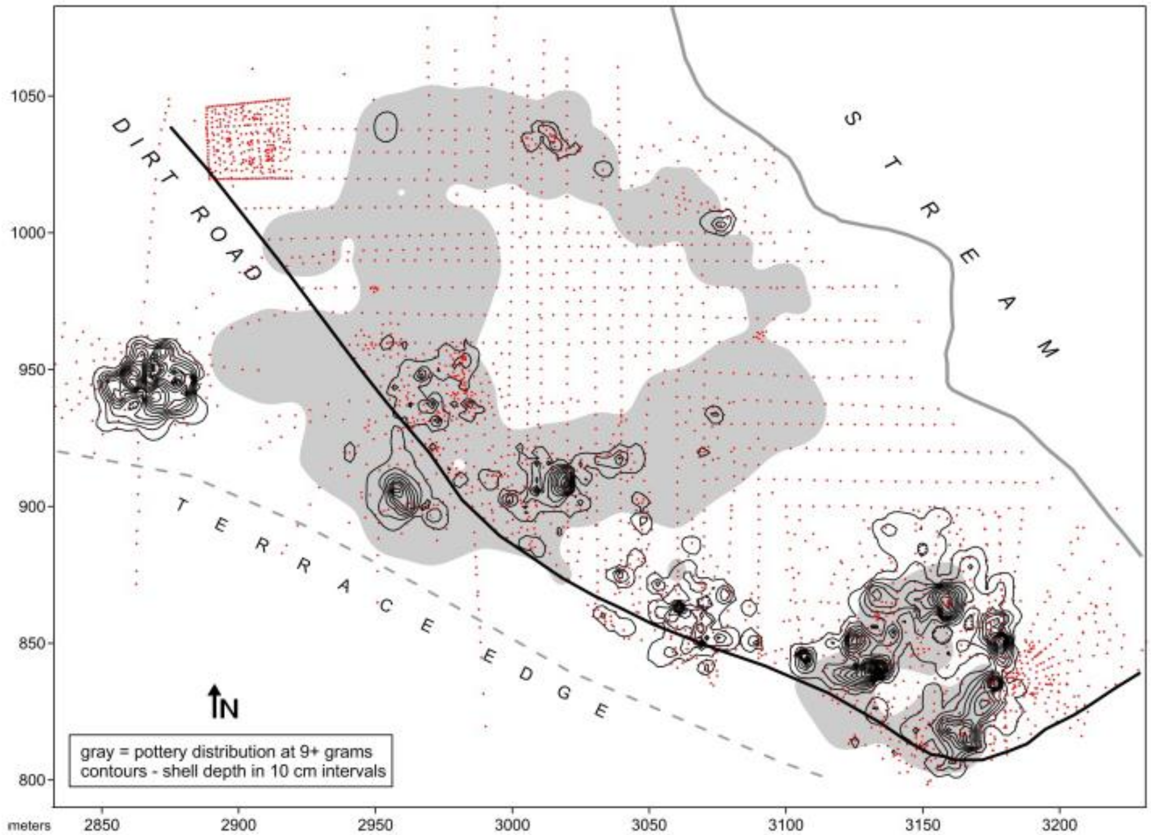

Figure 2 Map showing the pottery and shell distribution at the Hare Hammock complex. Probes for shell were taken around the assumed locations of 8By30 and 8By31. Contours are displayed using 10 cm intervals, and represent shell thickness as measured by probes (adapted from Russo et al., 2009).

The burial mounds at Hare Hammock (8By30, 8By31) were first located and excavated by Moore in 1902 (Moore, 1902), and later revisited by him in 1918 (Moore, 1918). In 2007, Russo and colleagues attempted to relocate Moore's smaller mound at Hare Hammock, 8By31, by conducting a systematic shovel-test survey in the area east of burial mound 8By30. A total of 154 shovel tests were placed, 109 of which were positive for pre-Columbian artifacts. A systematic survey was also conducted at 20-meter intervals in the far eastern portion of the survey area. During the surveys, two new ring-midden sites, 8By1347 and 8By1359 (Harrison Ring), were identified (Russo et al., 2009) (Figure 2).

At Harrison Ring, 97% of the decorated sherds were found to be pottery types produced during the Swift Creek period. These included both Swift Creek Complicated

Stamped and Residual Plain with podals (Russo et al., 2009). At Harrison Ring, several radiocarbon assays have been undertaken and show general age agreement with expectation with the occupation of Swift Creek peoples in Florida (Table 1 and Appendix A, Table 1). Based on these findings, it has been interpreted by archaeologists that the ring midden, or village/ceremonial center (8By1359), was first occupied around A.D. 400 by Swift Creek people (Russo et al., 2009; 2014). Subsequently, Swift Creek descendants increased the intensity of their living at Hare Hammock as supported by the construction of a burial mound (8By31) adjacent to their living area, as well as the placement of exotic objects in burial pits within the plaza. Radiocarbon ages from the midden and from the adjacent burial mound suggest that the most intense use of the sites occurred from between A.D. 500 to about A.D. 700. Subsequently, radiocarbon ages suggest that a new ring midden (8By1347) was constructed (Russo et al., 2009; 2014).

The radiocarbon dates taken at Harrison Ring and reported in Table 2 below include two shell species in which a marine reservoir correction (ΔR) was made. This local marine reservoir correction was made by measuring the difference in age between two pairs of contextually similar paired samples of shell with other datable material such as bone or charcoal from the same archaeological context (Shanks and Byrd, 2012). This reservoir correction was based on the pairing of only two samples from Wild Goose Lagoon. The validity of these corrections relies on a number of assumptions including undisturbed context of the samples and coincident deposition of the paired materials. Despite the number of assumptions that were involved in creating this local reservoir correction and the limited number of sample pairs, the corrected dates appear to be consistent with those radiocarbon dates taken from other materials, and expectation based on the ceramic assemblages at the Harrison Ring complex (Shanks and Byrd, 2012).

Table 2 Radiocarbon dates taken from Harrison Ring (8By1359) (Adapted from Russo et al., 2009; 2014)

Excavation unit / Feature (F)	**Material**	**Artifact**	**Conventional age BP**	**Calibrated age AD (2σ)**	**Calibrated age (cal BP)* (2σ)**
ST149	Shell	*P. gigantea*[1]	1470 ± 50	470 – 790	1545 – 1225
EU 7, F1	Bone	Turtle	1020 ± 30	780 – 1000	1235 – 1015
EU 7, F1	Bone	Turtle	1190 ± 30	670 – 770	1345 – 1245
EU 7, F6	Wood	Charcoal	1490 ± 30	550 – 650	1465 – 1365
EU 11, F8	Shell	*B. sinistrum*[2]	1410 ± 30	510 – 700	1505 – 1315
EU 11, F8	Bone	Turtle	1320 ± 30	590 – 670	1425 – 1345
EU 28, F12	Shell	*B. sinistrum*[2]	1340 ± 30	590 – 770	1425 – 1225
EU 28, F12	Bone	Turkey	1220 ± 30	650 – 770	1365 – 1245
EU 29, F13	Soot	Swift Creek Complicated Stamp	1540 ± 30	420 – 570	1595 – 1445
Range			**1570 – 990**	**420 – 1000**	**1595 – 1015**

* The calibrated radiocarbon age (cal BP) reflects the time before 1950.
1. ΔR 121 ± 52
2. ΔR 52 ± 32

At the three excavation units in Harrison Ring studied in this project, EU 27, 28 and 29, the ceramics have been classified as Swift Creek, exhibiting the classic scalloped, pie-crust, and ticked rims on both the plain and decorated sherds (Dengel 2014, pers. comm.). Decorated sherds are all from the Swift Creek series as defined by Willey (Willey, 1949). Other artifacts that were found in these excavation units are outlined in Table 3.

Table 3 Artifacts recovered from the archaeological excavation done in June 2013 near the area where OSL samples were collected

Excavation Unit & Artifact	Depth below surface (cm)	Other Comments
EU 27		
Woodland point	67	Within feature 20
Woodland triangular	76	Within feature 20
Half rose quartzite celt	42	Within feature 12
EU 28		
Quartz coble	37	Within feature 12
Groundstone	60	Within feature 12
Quartzite pecking stone	49	Within matrix
Worked quartzite cobble	67	Within feature 12
Kirk point	67	Within feature 12
EU 29		
Siltstone engraved gorget	46	Top of feature 13
Projectile point	46	Top of feature 13

1.2.3 Al_2O_3:C Dosimetry

Al_2O_3:C dosimeters have been studied and used widely for use in radiotherapy applications (eg. Botter-Jensen et al., 2003; Polf et al., 2003). These dosimeters have been applied by Kalchgruber et al. (2003) to sediments to determine dose-rate variation in samples, but at the time only the full dose-rate to the dosimeters could be determined. The application of the Al_2O_3:C dosimeters was later refined in study by Kalchgruber and Wagner (2006) who were able to separate the beta and gamma dose rate components by using a pair of dosimeters: one wrapped in thin foil measuring beta and gamma components, and the second packed in a copper container measuring the gamma component. This dosimetric technique was applied to both homogenous and inhomogenous sediments and compared successfully against results obtained using Ge- and on-site NaI-gamma dosimetry.

CHAPTER 2: STUDY AREA

2.1 Geological Setting

Tyndall Air Force Base (TAFB) lies on a 5 km wide peninsula between the Gulf of Mexico and the eastern arm (East Bay) of St. Andrew Bay. The TAFB peninsula and its associated barrier islands and spits separate the bay system from the Gulf of Mexico (Figure 3). During the Pleistocene, multiple periods of sea level rise and decline resulted in the opening and closing of the bay, alternating its salinity from fresh to marine in the process. Over the last 5000 years, the watershed has been largely estuarine (Russo et al., 2009).

The geologic formations that form TAFB's land surfaces are Quaternary and Holocene sedimentary deposits representing onshore, near shore, and offshore environments. These marine terraces, defined as the Gulf Coastal Lowlands, are gently sloping plains that extend from the interior highlands to the coast (Puri and Vernon, 1964). TAFB falls within two physiographic subdivisions: Beach Dunes/Wave-cut bluffs and Flatwoods Forests (Musgrove et al., 1965). The Beach Dunes/Wave-Cut Bluffs subdivision occurs along the Gulf of Mexico and is marked by sand dune deposits and bluffs subject to rapid formation change and erosion. Characteristic landforms include barrier islands, coastal ridges, estuaries, lagoons, relict spits and bars, and sand-dune ridges (Schmidt and Wiggs-Clark, 1980). The Flatwoods Forests subdivision consists of slightly rolling to flat land located on terraces below 70 feet ASL. Characteristics of this subdivision include some well-drained areas as well as areas with perennial swamps (Schmidt and Wiggs-Clark, 1980).

The Tyndall Air Force Base lies on the Silver Bluff and Pamlico marine terraces. The Silver Bluff terrace, dating to about 5000 to 4000 B.P., extends from sea level to approximately 1 to 3 m ASL. (MacNeil, 1950). The older Pamlico terrace extends from approximately 3 to 8 m ASL. TAFB has a maximum elevation of less than 10 m ASL, and therefore the majority of its superficial geology consists of the Silver Bluff and Pamlico formations (MacNeil, 1950).

Southeast of the main peninsula landform that houses most of TAFB, lie two NW-SE trending thinner peninsulas (Raffield & Crooked Island, Figure 3), which are situated outbound of Harrison Ring. These sandy spits are most likely of Holocene age, like all other sandy spits in the area further southeast (eg. St. Joseph Peninsula, Rink and Lopez, 2010).

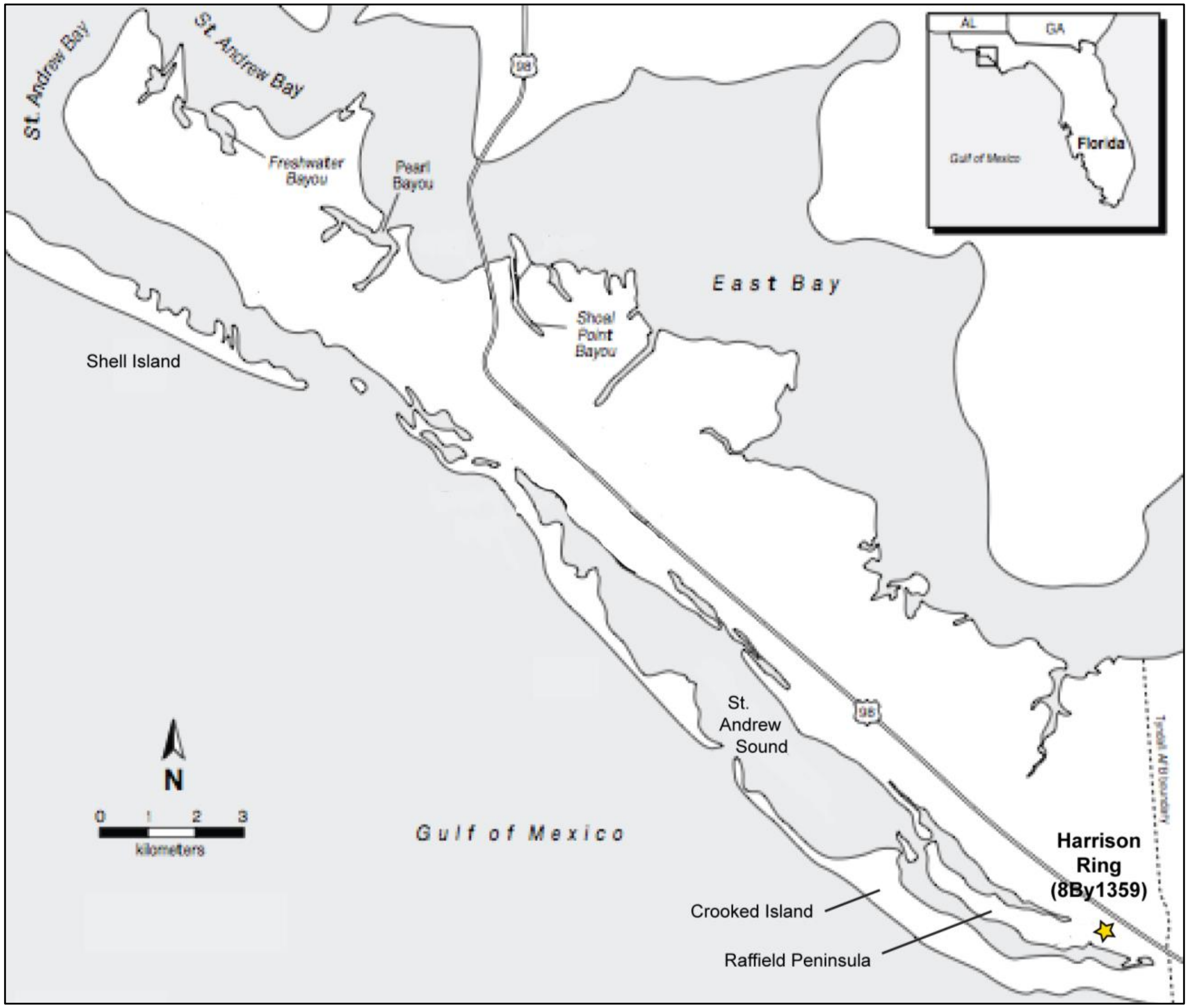

Figure 3 Location map showing the Harrison Ring site (marked with a star) located at Tyndall Air Force Base, Panama City, Florida (adapted from NOAA, 1997).

2.2 Climate

The local climate consists of a long, warm and humid summer climate from May to October and a mild to cool winter (Duffee et al., 1984). Prevailing winds generally blow from the north or northwest in the winter, and in the south and southwest during most other times of the year. Typical annual precipitation is approximately 60 inches, with the wettest periods ranging from July to September and the driest from October to December (Russo et al., 2009).

2.3 Flora and fauna

The vegetative communities on TAFB are successional forest types consisting of planted pines, natural longleaf pines and coastal hammock forests. In prehistoric times, the forests were likely dominated by fire sub-climax communities of longleaf pines with coastal hardwood oak-hickory-magnolia hammocks where forests were protected from fire on better-drained soils (Braun, 1950). Recent land clearing and use of lands for pasture and agriculture has eliminated these natural forest communities.

The most common mammal species in the area include white tailed deer, rabbit, squirrels, opossum, and raccoon. Bird species include wild turkey, quail, wood duck and numerous songbirds. Common reptiles include the terrestrial gopher tortoise, box turtle, and various snakes (Russo et al., 2009).

2.4 Archaeological Sites near Harrison Ring dated with OSL

Several important coastal prehistoric archaeological sites are found near the coast of the Florida Panhandle. There are two archaeological sites that have been dated with OSL that are in close proximity to Harrison Ring. Richardson’s Hammock, a shell midden located at the southern end of St. Joseph Peninsula has been dated to A.D. 505-705. This was shown to be consistent with the chronology of Early Weeden Island culture. In this study, Lopez (2007) has cited symmetrical equivalent dose distributions with only a small positive skew (< 1.13), and overdispersion values that do not increase with measurements on smaller mask sizes. Taken together, these results suggested that the dated quartz was well bleached and likely not affected by post-depositional reworking processes. Dose rates at the site were low and ranged from 257.6 – 518.2 μGy/a with a dominant cosmic dose component.

Located further north on St. Joseph’s peninsula, another shell midden known as the Old Cedar site has also been dated to 940 ± 100 a using OSL (Thompson et al., 2007). Old Cedar is well-known for its conch shell tool assemblage, which is uncommon in northwest Florida archaeological sites. The OSL age of the midden was dated to the Late Weeden Island period, consistent with expectation based on the artifact assemblages seen at the site. No evidence of post-depositional mixing or incomplete bleaching was present in these samples, although Thompson et al. (2007) suggest that the small positive skew in the samples may have been a result in natural variations due to inhomogeneities in the dose rate. Dose rates at the site were low and ranged from 244.1 – 435.6 μGy/a with a dominant cosmic dose component.

CHAPTER 3: INTRODUCTION TO LUMINESCENCE DATING

3.1 OSL Theory

Minerals, such as quartz and feldspar, contain various types of defects within their crystal lattices that cause electrons to become trapped. These defects, include those formed by elemental substitution (eg. Ti replacing Si in quartz) or by a negative-ion vacancy (Rhodes, 2011). After these minerals are deposited and buried, they are subjected to low levels of ionizing radiation that are a result of the radioactive decay of elements such as uranium, thorium and potassium, as well as by cosmic rays. This ionizing radiation provides energy that causes electrons in the crystal lattice of these minerals to become excited and move from the valence band into the conduction band (Rhodes, 2011). A small proportion of these electrons may become trapped at defects in the energy gap between the valence and conduction bands. Electrons accumulate in these traps over time. The depth of a given trap below the conduction band determines the stability of the trap and how long electrons can be stored (Rhodes, 2011).

Upon exposure to sunlight or heating, electrons are ejected from their traps and may recombine with a luminescence center. When this occurs, the electrons lose the energy that was gained during irradiation, some of which may be emitted in the form of photons (Figure 4). In the simplest scenario, the light emitted is proportional to the amount of trapped charge, and therefore represents the amount of energy that the mineral has accumulated since burial. Exposure to sunlight reduces the trapped charge population in the mineral, and acts as a “clock-resetting” event (Rhodes, 2011).

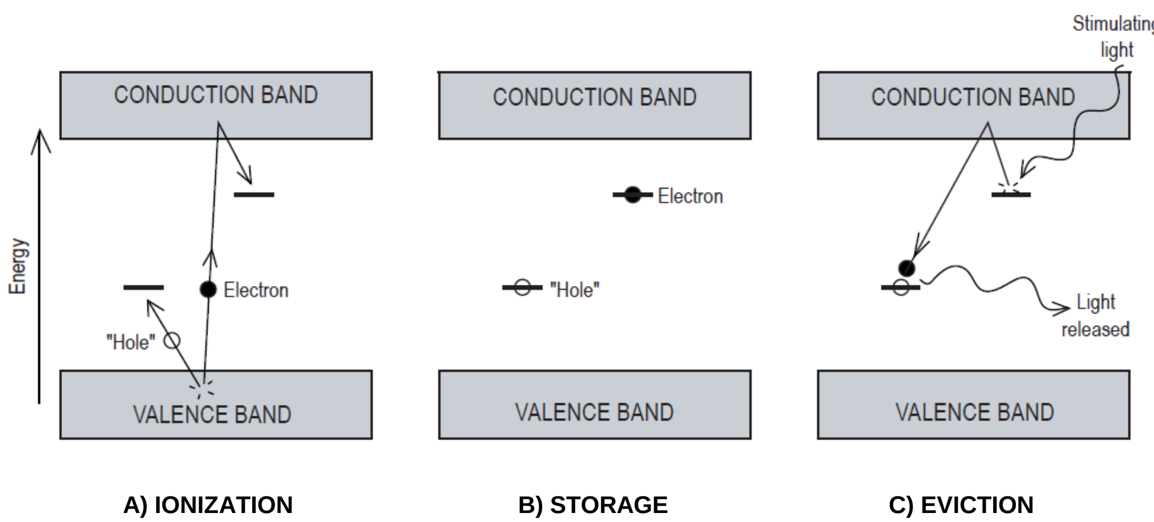

Figure 4 Schematic of the trapping of electrons in a crystal defect. (a) Ionization: exposing the mineral to radiation provides energy that causes electrons to become excited, (b) Storage: an electron becomes trapped, leaving behind an electron “hole”, (c) Eviction: Light stimulation frees the electron from its trap where it recombines with a luminescence center to produce photons (after Aitken, 1985).

In practice, after the sediment is collected, it is stimulated by light in the laboratory and these minerals release the energy in the form of photons (luminescence). Laboratory measurements are used to calculate the amount of laboratory radiation that is equivalent to the amount of absorbed ionizing radiation received in nature, which is also known as the equivalent dose (D_E, measured in grays (Gy), which represents 1 joule of energy/kilogram). When divided by the environmental dose rate, which represents the rate at which the sample received radiation through time, the luminescence age of the sample can be calculated:

Equation 1

$$Age\ (years) = \frac{Equivalent\ dose\ (Gy)}{Dose\ rate\ (\frac{Gy}{year})}$$

3.2 Laboratory measurement of OSL

In the laboratory, stimulation with light is used to release the trapped charge stored within minerals, and is termed optically stimulated luminescence (OSL). In quartz, the luminescence signal decays exponentially. The initial rapid decay (dominant fast component) is a result of luminescence being emitted from traps that are easy to bleach. The subsequent slower decay (medium and slow components) is the result of luminescence emitted by traps that are not as easily bleached (Aitken, 1998).

The wavelength of light chosen to stimulate the minerals is required to be significantly different compared to the emission wavelength of the mineral (Figure 5). Quartz OSL has a peak emission of between 365-380 nm (near-UV), and typically blue LEDs (light emitting diodes) with emission centered near 470 nm are used for stimulation. A filter is attached to the photomultiplier tube, and acts to prevent light from the stimulation source from being detected, while allowing UV light produced from quartz stimulation to pass through the detection window. A Hoya-U340 filter is commonly used when stimulating with blue LEDs (Rhodes, 2011).

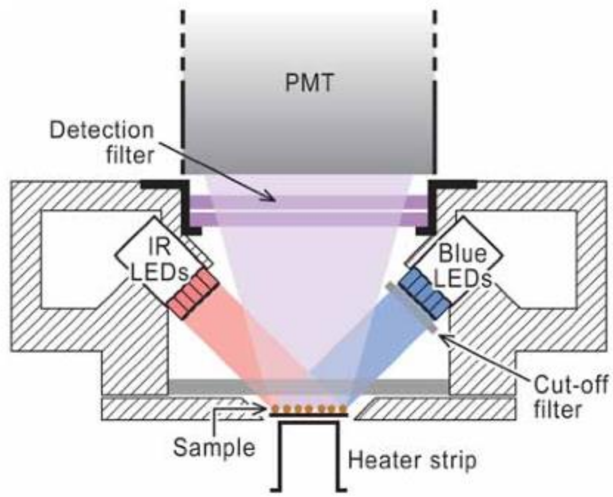

Figure 5 A schematic of the standard Risø OSL unit containing blue (470 nm) and IR (875 nm) LEDs (Bøtter-Jenson et al., 2010).

Infrared LED's, which have a peak emission centered around 875 nm, can also be used as a method of stimulation. The luminescence signal emitted from this stimulation, termed infrared stimulated luminescence (IRSL), is most frequently observed from feldspars. Quartz does not emit an IRSL signal at room temperature, and this fact can be used to check the purity of the quartz for OSL measurements.

3.3 Single-aliquot regenerative dose (SAR) protocol

The single-aliquot regenerative dose (SAR) protocol is a commonly used method for determining the equivalent dose (D_E) of a sample (Murray and Wintle 2000, 2003). The SAR protocol is composed of a series of cycles that are outlined in Table 4. In the first cycle, the natural luminescence signal (L_N), which represents the luminescence signal produced by the radiation that the sample was exposed to in nature, is measured. Following this measurement, a small known dose of laboratory radiation is applied (known as a test dose), and after a cut-heat, the OSL signal is measured. After that, another dose called a given dose is regenerated, and measured after a preheat (L_1). Each subsequent cycle gives a different regenerative dose (ie. 20 Gy, 40 Gy, etc.) followed by an OSL signal measurement (L_2, L_3, etc.), which will ultimately build a growth curve (Figure 6). Each OSL measurement is always preceded by a preheat, which acts to remove any unstable electrons from shallow traps. The cut heat (heating prior to the test dose), is typically performed at a temperature similar to or lower than the preheat. After the measurement of every test dose, an illumination step at high temperature is performed in order to remove any remaining trapped charge before the next measurement cycle (Murray and Wintle, 2000, 2003) (Table 4).

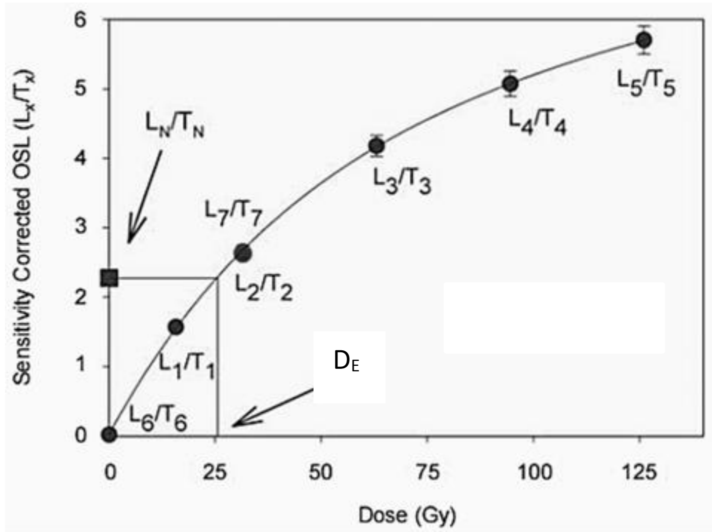

Figure 6 A growth curve used for equivalent dose determination. During a typical single-aliquot regenerative dose (SAR) sequence, the natural or regenerative dose OSL (Lx) is corrected by the OSL response to a test dose (T_x). For each aliquot measured, the natural OSL (L_1/T_1) is compared to the growth curve created by the regenerative-dose OSL to obtain a D_E estimate (Duller, 2008).

The luminescence sensitivity of an aliquot (small portion of a sample mounted on an aluminum disc) is known to change over the course of a SAR measurement sequence. As a consequence of this, it is necessary to monitor the sensitivity change for each OSL measurement. This is accomplished by giving a known dose, called a test dose, following each measurement cycle. Any sensitivity change is recognized by comparing the natural and regenerative-dose measurement to the subsequent sensitivity measurement (L_x/T_x). These points plot as a growth, or dose-response curve, with typically three to five used to obtain an appropriate curve. The D_E is determined by finding the intercept of the natural luminescence signal with the growth curve (Murray and Wintle, 2000, 2003).

Table 4 A typical SAR sequence used for quartz OSL measurements (Murray and Wintle, 2000)

Step	**Treatment**	**Observed**
1	Natural or given dose, Di	--
2	Preheat (160-300 °C for 10 s)	--
3	Stimulate for 40 s at 125 °C	Li
4	Give test dose, Dt	--
5	Cut heat (160-300 °C)	--
6	Stimulate for 40 s at 125 °C	Ti
7	Stimulate for 40 s at 280 °C	--
8	Return to step 1	--

The SAR protocol includes several built-in checks that can be used to assess the behaviour of each aliquot. The recycling test assesses the effectiveness of the SAR protocol to correct for changes in sensitivity. This is done by comparing the final regeneration dose response to the first regeneration dose response. If the ratio between the two sensitivity-corrected luminescence signals, known as the recycling ratio, is equal to 1, this suggests that the SAR protocol was able to correct for sensitivity changes that occurred over the measurement cycles. In practice, a ratio between 10% of 1 (ie. 0.9 to 1.1) is considered acceptable. A ratio greater or less than this implies that the SAR protocol is likely to be inappropriate for use with the samples.

Another test is known as the recuperation test. This test is performed by introducing a zero dose within the regenerative sequence. Theoretically, this sensitivity corrected signal, L_0/T_0, should be close to zero. A value above zero indicates that there is an aspect of the signal which is not being depleted by light stimulation, which may be related to thermally transferred charge. In practice, a small signal is very commonly observed, but is considered insignificant if it is less than 5% of the natural signal (L_N/T_N).

CHAPTER 4: METHODS

4.1 Sample Collection & Preparation

A total of 17 sediment samples were collected during June 2013 on the Tyndall Air Force peninsula (N 29.96838, W 85.45601; approximately 5 m ASL) in three adjacently located excavation units: EU 27, EU 28 and EU 29 (Figure 8). Eleven samples from EU 27 were collected at 10 cm intervals down the profile (referred to as the stratigraphic section) exposing cultural and geological horizons, and the remaining samples were taken from exposed archaeological features. These archaeological features, interpreted as infilled pits, were distinguished based on their dark colouration and relatively high concentration of artifacts (Dengel 2014, pers. comm.). During sample collection, the exposed walls were cut back vertically in order to clean the exposure and avoid sampling of loose, light-exposed material. Samples were collected by inserting copper tubes horizontally into the vertically exposed stratigraphy (Figure 7). When filled with sediment, they were carefully removed from the profile and any unfilled space in the tube was packed with aluminum foil to ensure that no mixing of the sediment occurred. The sample tube was then sealed with opaque black tape on either end. Each tube was subsequently wrapped in aluminum foil to maintain light-tight conditions.

Figure 7 A generalized view of the stratigraphy from the west profile of EU 27 and the approximate locations of the three major soil horizons that are present. OSL samples from the stratigraphic section were taken from approximately the same location as the tape measure.

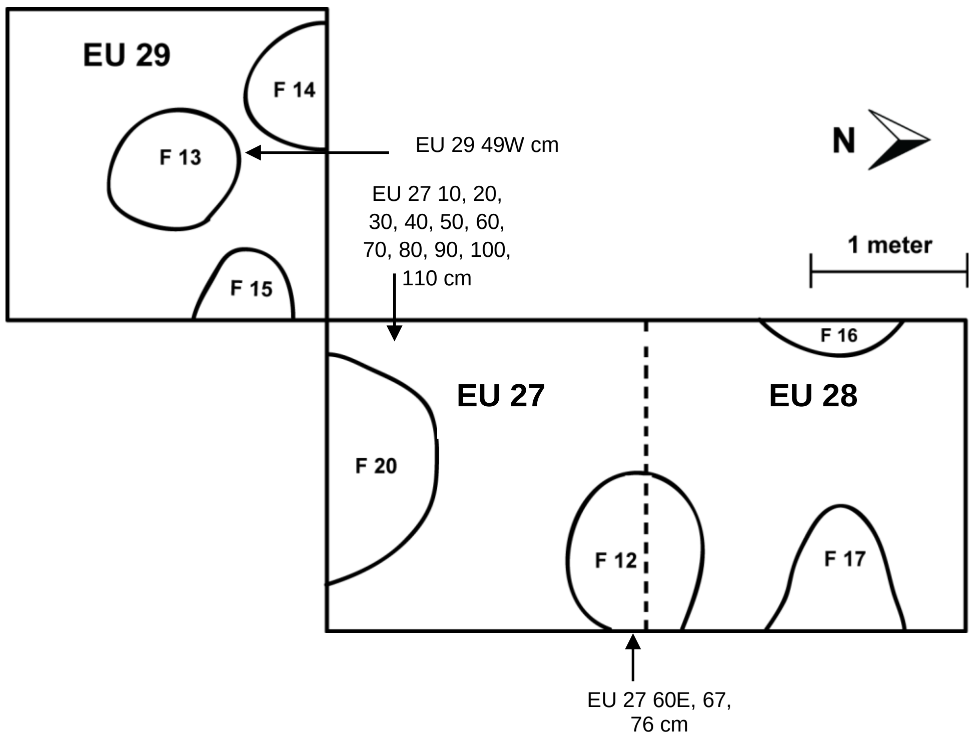

Figure 8 A plan view of the study site and the approximate locations where samples were collected in each of the excavation units EU 27, EU 28 and EU 29.

After transportation back to the AGE Laboratory (McMaster University), in a darkroom laboratory under low orange light, the sample tubes were opened and the sediment at either end of the tube was removed to prevent contamination of the working sample with light-exposed quartz grains. Following oven drying (~60 °C), the samples were weighed, moisture content was calculated and ~1 g of whole sediment was collected for NAA/DNC. A series of chemical treatments were then completed on the remaining sediment. The samples were first treated with 10% HCl and 30% H_2O_2 to remove carbonates and organic material respectively. Standard dry sieve methods were used to obtain the 212-150 µm grain size fraction. Heavy minerals were then removed from the 212-150 µm grain size fraction for each sample using Lithium polytungstate (2.75 g/mL). The remaining quartz grains were treated with 40% HF for 40 minutes to etch the quartz and remove any remaining feldspar from the sample. The samples were then immediately treated with a 10% HCl solution for 15 minutes.

4.1.2 Multi-grain and single grain disc preparation

Multi-grain aliquots were prepared on 9.8 mm-diameter stainless-steel discs. The number of grains mounted on discs varied between measurements. Grains were loaded onto the stainless steel discs by applying Silkospray through a 3 mm or 0.5 mm-diameter mask. Aliquots sizes were of ~170 grains and ~15 grains respectively.

Single-grain measurements were made using aluminum discs that contain 100 holes arranged in a 10 × 10 grid. Each hole had a diameter of 300 μm and was 300 μm deep. Grains were placed in each hole by brushing grains over the surface of the discs. To ensure that there was only one grain per hole, each one was visually checked under a light microscope using red lighting.

4.2 Dosimetry

Dosimetry at the study site was performed using two techniques described below:

1) Aluminum oxide dosimeters (Al_2O_3:C)

Dosimetry was conducted using highly radiation-sensitive Al_2O_3:C single-crystal chips using protocols based on work by Kalchgruber and Wagner (2006). The Al_2O_3:C chips were placed within OSL sampling locations at the back of the hole that the copper sediment containing tube was extracted from. To obtain separate measurement of beta and gamma dose rates, burial dosimeters were buried on the end of wood dowels in pairs: one with stainless steel casing, and one without casing, but wrapped only in electrical tape. Burial dosimeters with a stainless steel casing measured combined gamma and cosmic doses. Burial dosimeters without a steel casing absorbed beta, gamma and cosmic doses. The dosimeters were left buried in the profiles at Harrison Ring for 341 days to accumulate the environmental dose, after which they were excavated and sent to North Carolina University for dose measurement by Dr. Regina DeWitt. These dosimeters were transported with 8 evenly distributed travel dosimeters which were zeroed before transport, and whose function was to record the dose accumulated over the course of transport to the lab and storage in the lab before measurement.

Following burial the thermoluminescence (TL) signal of the dosimeters was measured using a Risø TL-DA-15 with heating up to 400 °C at a rate of 5 °C/s using Hoya U-340 filter. The signal was integrated under the main dosimetric peak occurring near 200 °C. A signal from a 5 s given dose was used to calibrate for different sensitivities between Al_2O_3:C chips.

For calibration, another set of dosimeters were buried in reference soil with a well-known dose-rate (Nussi, Antoine et al. 2001; Kalchgruber and Wagner, 2006) for 159 days. There was not enough material for full 4π geometry, and thus the gamma dose was calibrated using a different method. The steel encased dosimeters were irradiated with a ^{60}Co gamma source at the Nuclear Reactor Program at North Carolina State University, and the absorbed gamma and cosmic dose was measured using a ^{90}Sr beta source attached to the Risø that was calibrated against these dosimeters. The doses were measured using the travel-corrected signals from the travel dosimeters. The result was the gamma + cosmic dose absorbed in 341 days of burial. The calculated cosmic dose rate from 341 days was subtracted from this value to obtain gamma only.

For burial dosimeters that were not encased in steel, beta radiation had been attenuated in the Al_2O_3:C chips and needed to be treated in a different matter. Dosimeters buried in the Nussi reference material was used to calibrate the reader for a mixed beta-gamma field, where gamma penetrated the chips fully, and beta is attenuated. Using this calibration, the combined beta + gamma + cosmic dose was measured. The known gamma and cosmic dose was subtracted from this to obtain the beta dose only.

2) Neutron activation analysis (NAA) and Delayed Neutron Counting (DNC)

Untreated subsamples of the original samples were used to determine the elemental concentrations of radioactive isotopes. Dose rates were based on neutron activation analysis (NAA) of ^{232}Th, ^{40}K and delayed neutron counting (DNC) analysis of ^{238}U, all conducted at the McMaster University Nuclear Reactor.

4.3 Luminescence Measurements

4.3.1 Multiple grain single aliquot measurements

OSL measurements were taken with the Risø TL-DA-15 luminescence reader fitted with a Hoya U-340 UV transmitting filter. Laboratory irradiations were performed using a ^{90}Sr/^{90}Y (beta) radioactive source attached to the Risø luminescence reader. The procedure for determining a sample's final equivalent dose was done in three separate steps:

1) **Initial D_E & feldspar contamination check**
   An initial D_E estimate was made by comparing the natural OSL signal of four aliquots to their OSL signal after a given dose. A second identical regenerative dose was applied to the same aliquots and the IRSL signal was measured. The range of D_E's were used to select the regenerative doses needed to determine the final D_E of each sample.

2) **Dose recovery & thermal transfer test**
   A dose recovery test was used to assess the best temperature (160 °C, 200 °C, 240 °C and 260 °C) at which a given dose can be recovered using the SAR protocol. Three aliquots were measured at each preheat temperature yielding a total of twelve aliquots per sample measured. The preheat temperature that produced a dose closest (within error) to the given dose was selected for use in the final D_E measurement. For selected quartz samples, a thermal transfer test was also carried out to determine the possible charge transfer from light insensitive shallow traps to light sensitive OSL traps due to the effect of high temperature treatments. This test was carried out by bleaching the samples using blue light stimulation for 400 s at 260 °C, with a pause of 2000 s, and subsequently measuring the natural signal at preheat temperatures 160 °C, 200 °C, 240 °C and 260 °C.

3) **Final D_E measurement**
OSL measurements were made on 48 aliquots for each measured sample using a 3 mm or 0.5 mm mask size. Measurements followed the SAR protocol, with the OSL signal integrated from channels 1 to 2 (the first 0.4 s), and the subtracted background integrated from the last 10 channels (the last 4 s) of the OSL decay curve.

Step	**Treatment**
1	Natural or Given dose, Di
2	Preheat (200 °C for 10 s)
3	Stimulate for 40 s at 125 °C
4	Give test dose, D_t
5	Cut heat (160-300 °C)
6	Stimulate for 40 s at 125 °C
7	Return to step 1

Each of the sensitivity-corrected regenerative-dose points (L_X/T_X) were used to construct a sensitivity-corrected dose-response curve, from which the sensitivity-corrected natural signal (L_N/T_N) was interpolated to produce a D_E estimate. Each dose-response curve was fitted with a single saturating exponential function.

Aliquots were rejected on the basis of the following criteria:

Criteria	**Limit**
Recycling ratio	> 10%
Recuperation	> 5%
Signal to background noise ratio	< 3:1
Test dose error	> 5%
Paleodose error	> 5%

4.3.2 Single grain measurements

Single grain OSL measurements were performed using an automated Risø TL-DA-20 luminescence reader fitted with a Hoya U-340 UV transmitting filter at the Desert Research Institute in Reno, Nevada, USA. Laboratory irradiations were performed using a $^{90}Sr/^{90}Y$ beta radioactive source attached to the Risø luminescence reader. Single grain OSL measurements were made using focused green (532 nm) laser stimulation. Measurements followed the SAR protocol, with the OSL signal integrated from channels 6 to 9, and the subtracted background integrated from channels 46 to 55 of the OSL decay curve.

Measurement Protocol:

Step	Treatment
1	Natural or Given dose, D_i
2	Preheat (200 °C for 10 s)
3	Green laser stimulation for 1 s at 125 °C
4	Give test dose, D_t
5	Cut heat (160 °C)
6	Green laser stimulation for 1 s at 125 °C
7	Return to step 1

Rejection Criteria:

Criteria	Limit
Recycling ratio	> 20%
Recuperation	> 5%
Signal to background noise ratio	< 3:1
Test dose error	> 20%
Paleodose error	> 30%

4.4 Equivalent dose determination

The equivalent doses for accepted aliquots in each sample were displayed graphically using a probability density function. A minimum age model (MAM3) after Galbraith et al. (1999) was used to isolate the D_E used for final age calculation for each sample and aliquot size. A σ_b value, determined based on results of dose recovery experiments, was added in quadrature to all D_E estimates to account for variability caused by instrumental error and intrinsic luminescent properties (Galbraith et al., 2005). For more details see footnotes in Table 5.

4.5 Age Determination

The ANATOL v. 2.0.52 software (Mercier, 2012) was used to calculate ages, uncertainties, and dose rates. This version of ANATOL incorporates the dose rate conversion factors of Guérin et al. (2011). External beta dose rates were calculated assuming secular equilibrium in the ^{238}U and ^{232}Th decay chains, and determined from sediment ^{238}U, ^{232}Th and K concentrations from neutron activation analysis and delayed neutron counting. The external gamma dose rate used for age determination was based on in-situ Al_2O_3:C dosimetry. All beta and gamma dose rates were corrected for the estimated water content during measurement. The external alpha dose was removed during the 40% Hydrofluoric acid pre-treatment, and thus did not contribute to the dose rate. Cosmic dose rates were based on calculations performed in R and modeled based on methods by Prescott and Hutton (1988), which incorporate energy release data from Adamiec and Aitken (1998). The cosmic-ray dose rate was calculated using a 2 g/cm^3 of overburden density and assuming a linear accumulation over time. Internal concentrations of 0.06650 ± 0.02194 ppm of ^{238}U and 0.11350 ± 0.04248 ppm of ^{232}Th were used based on Rink and Odom (1991) measurements for granitic quartz. Beta absorbed fractions were taken from Mejdahl (1979).

In addition to the errors on the equivalent doses, the following systematic errors were incorporated into each age calculation: a) ± 25% for moisture content; b) ± 2% for etching; c) ± 10% for cosmic-ray dose rate, and d) ± 10% global systematic error.

CHAPTER 5: RESULTS

5.1 Luminescence behaviour

5.1.1 Thermal behaviour

The influence of the preheat temperature on the D_E value was examined for all measured samples using a dose recovery test. Results from two samples, EU 27 30 cm (stratigraphic section) and EU 27 76 cm (archaeological feature) are shown in Figure 9. In all cases, the equivalent dose (D_E) appears to be independent of preheat temperature between 160 °C and 280 °C, but in general shows best agreement with a given dose at 200 °C. Recycling ratios and recuperation are also independent of preheat temperature. Results of a thermal transfer test are also shown in Figure 9 for the same two samples. Thermal transfer appears negligible for sample EU 27 30 cm over the range of pre-heats investigated. Thermal transfer is larger at higher preheats for sample EU 27 76 cm, with D_E's displaying much larger errors when compared to sample EU 27 30 cm. Dose recovery tests on single grains suggest that approximately 15% of the overdispersion in D_E can be attributed to natural variations in luminescence properties of the grains.

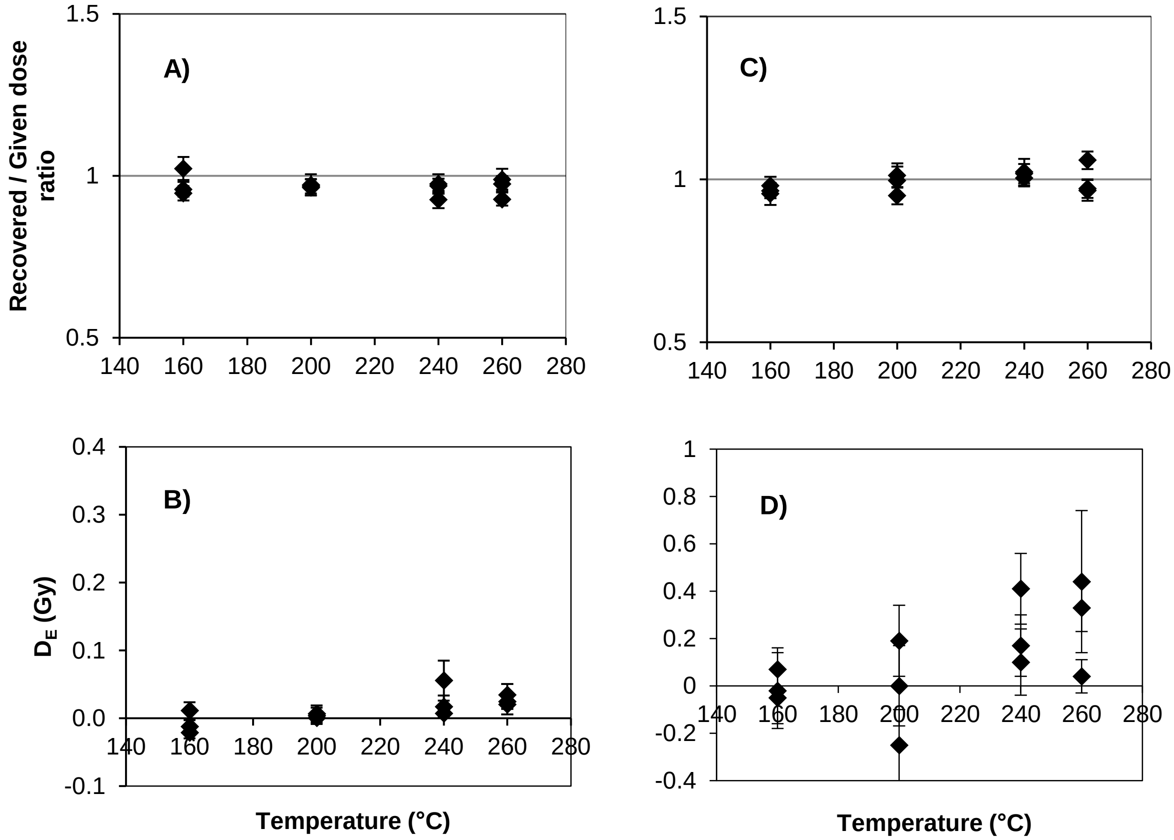

Figure 9 OSL thermal properties. (A) Dose recovery test for sample EU 27 30 cm taken from the stratigraphic section, (B) Thermal transfer test over the same range of preheat temperatures for EU 27 30 cm taken from the stratigraphic section, (C) Dose recovery test for sample EU 27 76 cm taken from an archaeological feature, and (D) Thermal transfer test for EU 27 76 cm taken from an archaeological feature.

5.1.2 Decay curves and dose response

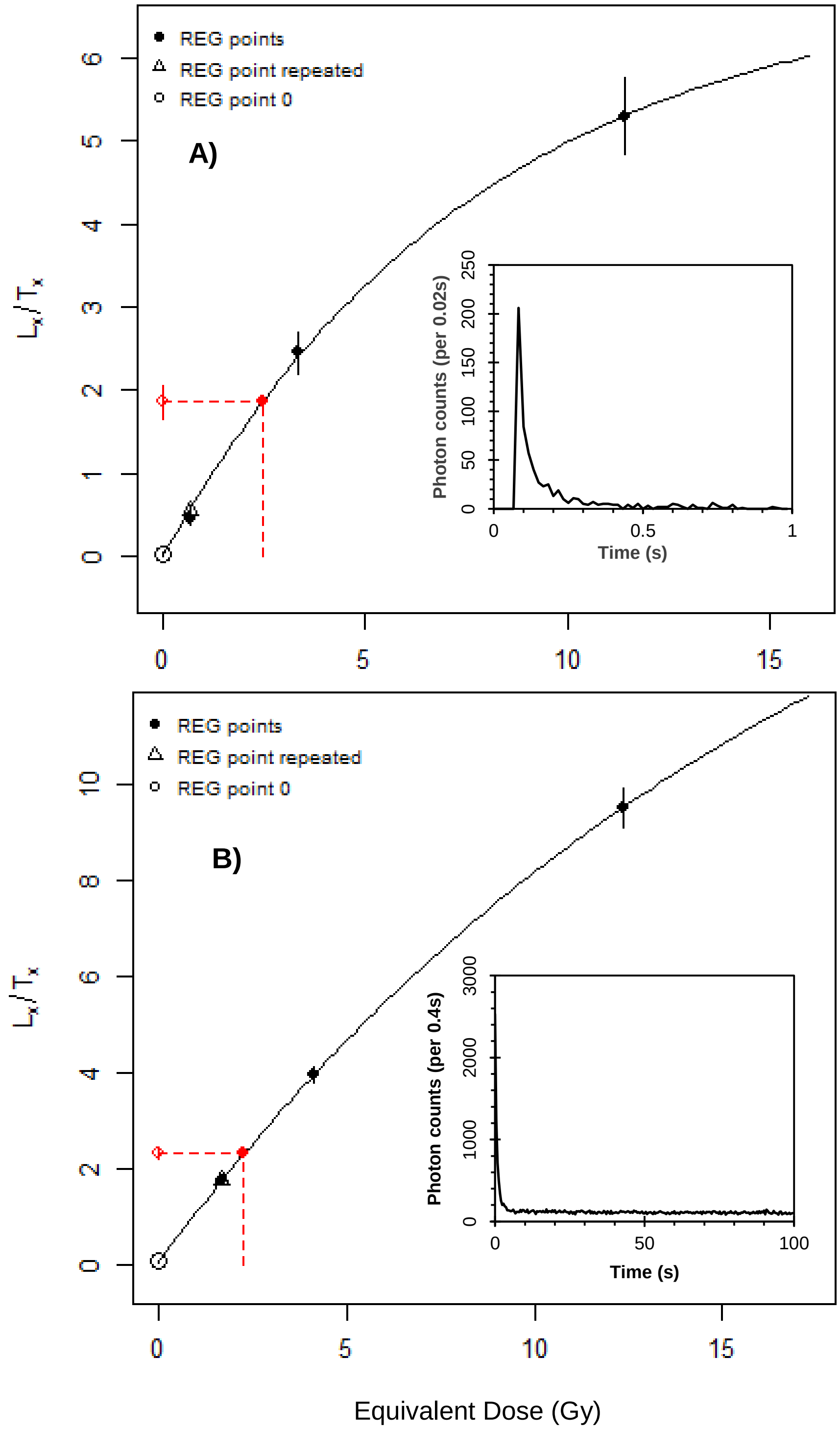

Figure 10 An example of a typical growth curves with corresponding decay curves (inset) for EU 27 30 cm using (A) single grains and (B) multi-grain (0.5 mm) aliquots. The red dashed line on the growth curves represents the equivalent dose. REG = regeneration point.

Figure 10 shows a representative OSL decay curve from samples measured using single grains and multi−grain (~15 grains) aliquots, together with each of their respective growth curves. The samples studied show rapid OSL signal decay, indicating that the signal is dominated by the fast component. No significant differences in terms of luminescence characteristics have been observed among the samples investigated here. The growth curve can be well represented by a single saturating exponential function. All natural signals lie well below the laboratory saturation level. Figure 10 also illustrates the general behaviour of the samples in the SAR protocol. Sensitivity changes occurring during the repeated SAR cycles are accurately corrected for, as is indicated by the ability to re-measure points on the dose-response curve (Figure 10, open triangles).

5.1.3 Cumulative light sum

A cumulative light sum has been plotted for samples throughout EU 27 in order to determine the contribution of luminescent grains in a multiple grain aliquot (Figure 11). This was accomplished by ranking the intensity of the natural luminescence signal produced (from single grain measurements) in order of descending brightness, and plotted as a function of the proportion of grains involved (Duller et al., 2000). If all grains were contributing equally, the cumulative light sum would plot as a 1:1 ratio. Based on the characteristics of their cumulative light sum, samples fall in to two major categories. In samples from the stratigraphic section, approximately 95% of the light sum is derived from 5-7% of grains. In samples collected from features, 95% of the light sum is derived from 10-15% of grains.

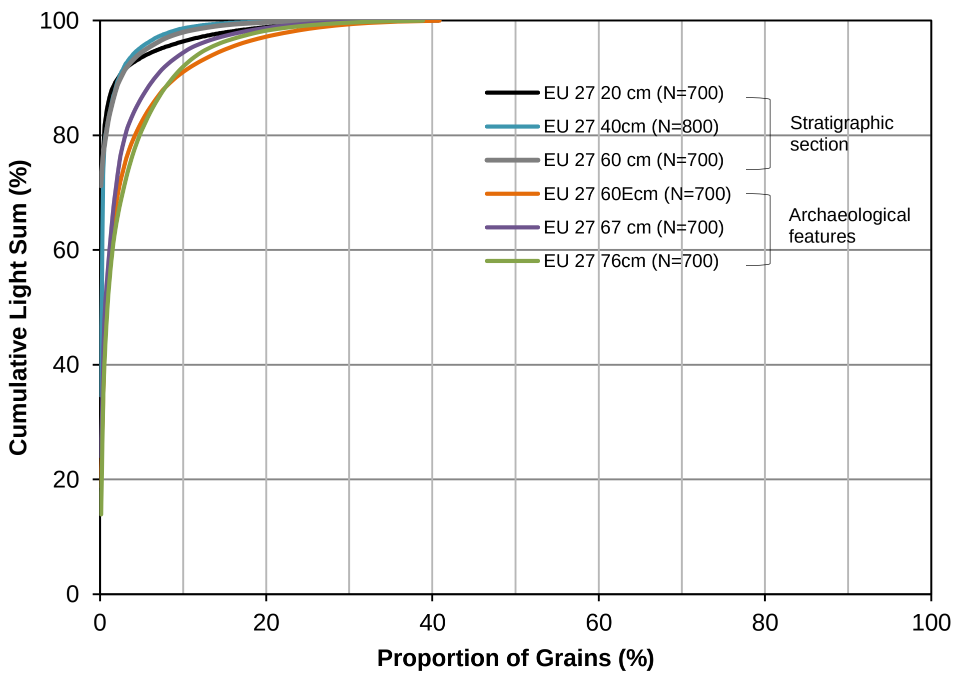

Figure 11 Cumulative light sum curves for selected samples in EU 27 at Harrison Ring.

5.2 Equivalent Doses

Equivalent dose distributions for all measured samples are presented as probability density plots in Figures 12 and 13. In addition, various statistical metrics for D_E distributions are presented in Tables 5 and 6. In general, samples from EU 27 have MAM3 D_E's that are statistically indistinguishable and therefore consistent between measurements on 0.5 mm aliquots and single grains. EU 27 10 cm, EU 27 60 cm and EU 27 76 cm are exceptions to this. Where measurements on 3 mm aliquots were carried out, MAM3 D_E's were largely overestimated when compared to either measurements on 0.5 mm aliquots or single grains. Overdispersion values range from 107% to 49% at the single grain level, 88% to 12% using 0.5 mm multi-grain aliquots, and 65% to 21% using 3 mm multi-grain aliquots. Dose distributions using any aliquot size appear to be positively skewed with an overdispersion significantly greater than that which is expected from intrinsic sources of variability (as estimated using a dose recovery test). These overdispersion values are typically largest in near surface samples, and decrease with depth in the profile. The overdispersion values are generally larger in single grain measurements compared to multi-grain measurements, which is expected based on the fact that single grain measurements remove any averaging effects between equivalent dose values. Equivalent doses appear to demonstrate multimodal distributions, which are most apparent at the single grain level.

Stratigraphic Profile

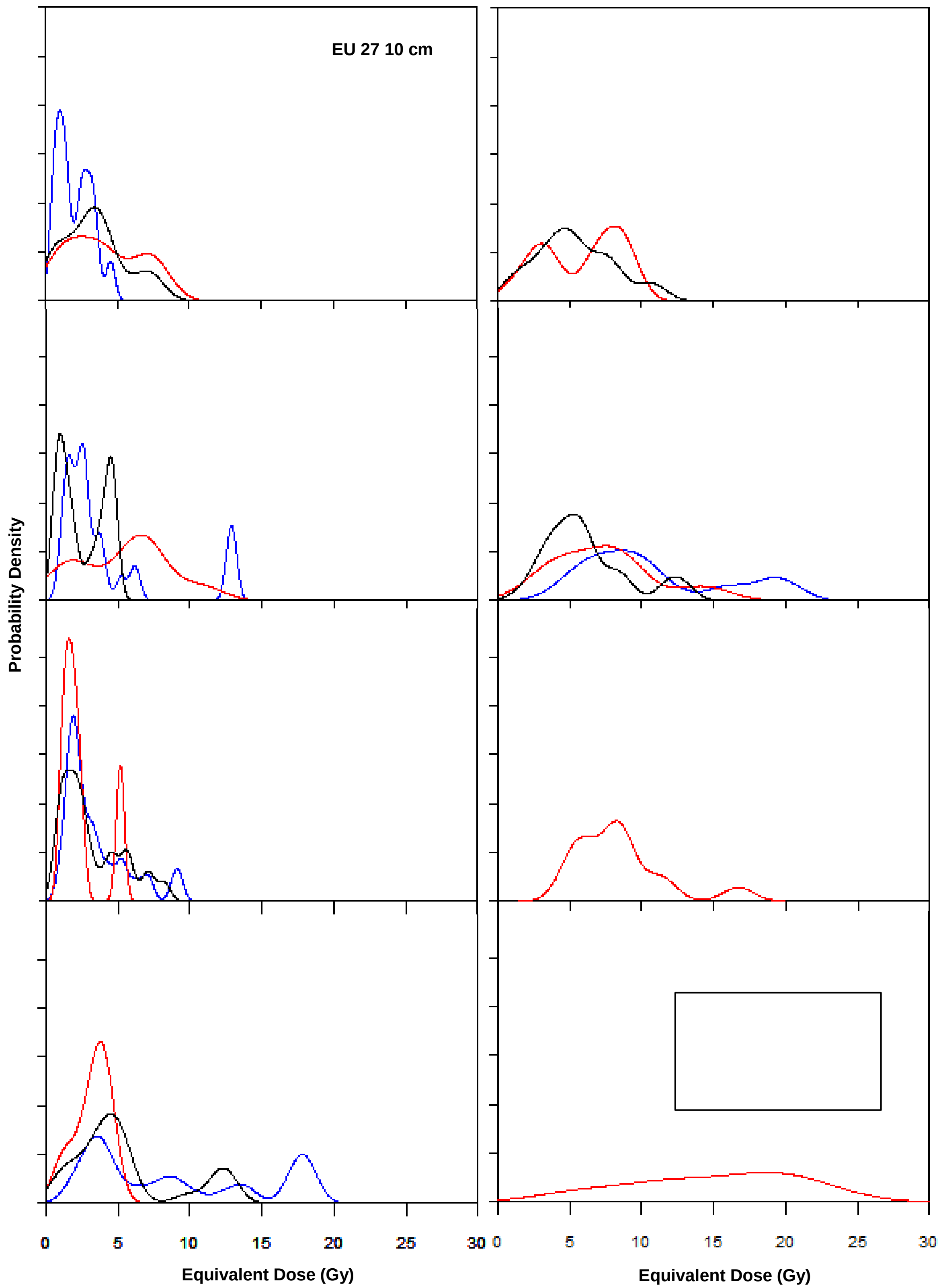

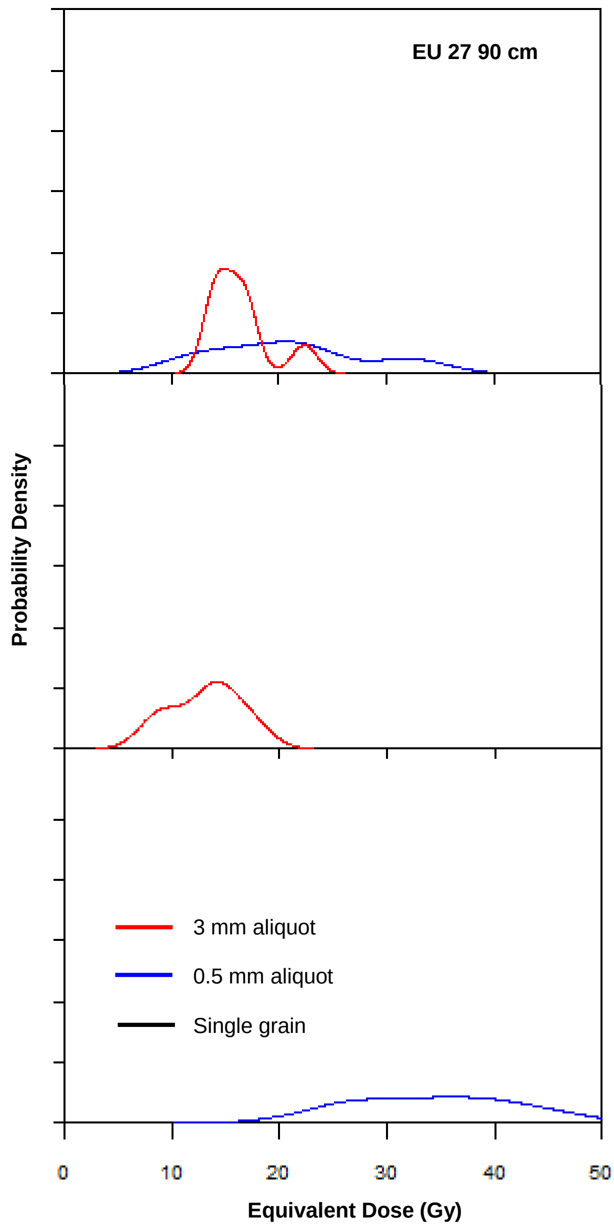

Figure 12 Equivalent dose distributions presented as probability density plots for the stratigraphic section of EU 27 at Harrison Ring. Results of 3 mm, 0.5 mm and single grain measurements are displayed.

Archaeological Features

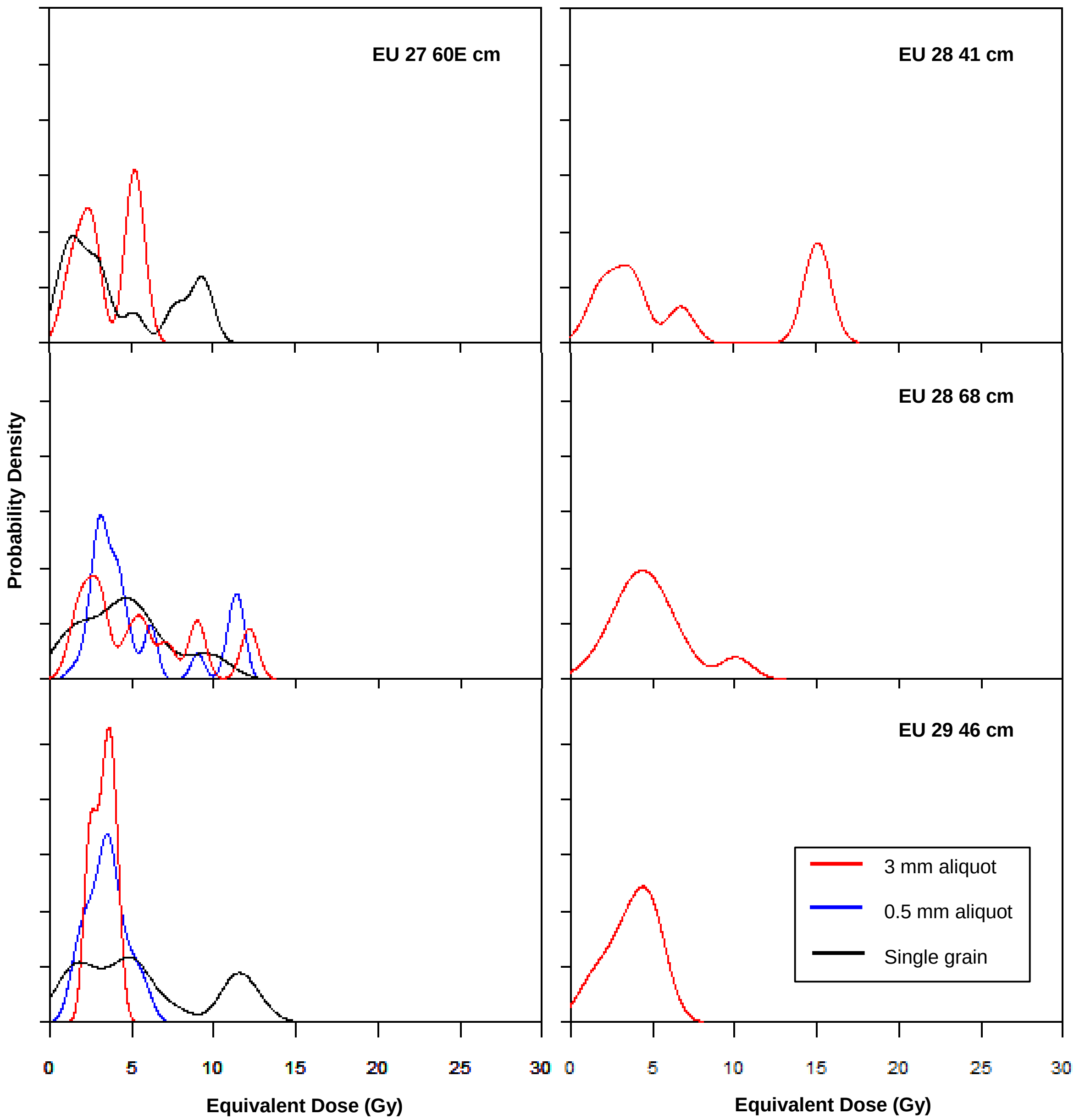

Figure 13 Equivalent dose distributions presented as probability density plots for all sampled archaeological features in EU 27, EU 28 and EU 29 at Harrison Ring. Results of 3 mm, 0.5 mm and single grain measurements are displayed.

Table 5 Equivalent dose characteristics for samples in EU 27, EU 28 and EU 29 at Harrison Ring

		3 mm aliquots				0.5 mm aliquots				Single grains			
Sample (Feature)	**Depth (cm)**	**N**	**MAM3 D_E Range (Gy)[1]**	**OD (%)**	**MAM3 D_E ± 1σ (Gy)[1]**	**N**	**MAM3 D_E Range (Gy)[1]**	**OD (%)**	**MAM3 D_E ± 1σ (Gy)[1]**	**N**	**MAM3 D_E Range (Gy)[1]**	**OD (%)**	**MAM3 D_E ± 1σ (Gy)[1]**
Stratigraphic Section													
EU 27 10 cm	10	48	0.3 – 4.5	65 ± 5	0.36 ± 0.03	7	0.7 – 7.3	85 ± 21	0.73 ± 0.11	16	0.17 – 7.15	107 ± 21	0.24 ± 0.07
EU 27 20 cm	20	48	0.9 – 12.9	49 ± 4	1.05 ± 0.06	18	0.8 – 10.8	88 ± 14	0.83 ± 0.06	35	0.6 – 4.6	61 ± 7	0.82 ± 0.11
EU 27 30 cm	30	47	0.9 – 9.1	51 ± 4	1.01 ± 0.06	12	1.1 – 5.2	40 ± 6	1.12 ± 0.13	35	0.7 – 8.2	60 ± 7	1.04 ± 0.13
EU 27 40 cm	40	48	1.4 – 18.2	62 ± 5	1.61 ± 0.11	11	0.8 – 4.5	58 ± 10	0.84 ± 0.13	38	0.6 – 12.3	66 ± 7	0.94 ± 0.15
EU 27 50 cm	50					8	0.9 – 8.7	70 ± 15	0.94 ± 0.19	47	0.5 – 10.7	71 ± 7	0.94 ± 0.14
EU 27 60 cm	60	48	2.7 – 20.6	43 ± 3	3.25 ± 0.22	11	3.3 – 14.2	45 ± 7	3.68 ± 0.31	39	1.0 – 12.9	49 ± 5	1.95 ± 0.28
EU 27 70 cm	70					20	4.7 – 16.7	31 ± 3	5.28 ± 0.4				
EU 27 80 cm	80					18	4.5 – 22.5	52 ± 6	4.90 ± 0.5				
EU 27 90 cm	90	47	8.0 – 35.3	35 ± 2	9.62 ± 0.61	7	14.0 – 22.4	12 ± 2	15.1 ± 1.17				
EU 27 100 cm	100					7	8.8 – 17.2	22 ± 3	11.85 ± 1.1				
EU 27 110 cm	110	39	20.0 – 47.8	21 ± 1	30.28 ± 1.09								
Archaeological Features													
EU 27 60E cm (F12)	60					14	0.9 – 5.7	56 ± 8	0.97 ± 0.11	28	0.5 – 9.5	75 ± 10	0.90 ± 0.17
EU 27 67E cm (F12)	67	48	1.3 – 11.3	45 ± 3	1.53 ± 0.10	26	1.0 – 12.2	57 ± 6	1.26 ± 0.15	31	0.7 – 10.3	76 ± 9	0.98 ± 0.17
EU 27 76 cm (F12)	76	45	1.2 – 6.1	37 ± 2	1.56 ± 0.10	7	2.4 – 3.9	15 ± 3	1.58 ± 0.11	45	0.7 – 12.6	75 ± 8	1.01 ± 0.15
EU 28 41W cm	41					12	1.27 – 15.07	65 ± 11	1.37 ± 0.22				
EU 28 68W cm	68					19	0.8 – 10.0	63 ± 8	0.93 ± 0.11				
EU 29 46W cm (F13)	46					7	1.0 – 5.1	58 ± 12	1.09 ± 0.17				

1. Minimum age model (MAM) D_Es calculated using a σb value of 0 for 3mm aliquots, 0.08 for 0.5 mm aliquots and 0.15 for single grains

Table 6 Summary of statistical measures for samples in EU 27, EU 28 and EU 29 at Harrison Ring

		3 mm aliquots			0.5 mm aliquots			Single grains		
Sample (Feature)	**Depth (cm)**	**N**	**Skewness**	**Kurtosis**	**N**	**Skewness**	**Kurtosis**	**N**	**Skewness**	**Kurtosis**
Stratigraphic Section										
EU 27 10 cm	10	48	1.22	3.59	7	0.81	2.01	16	1.10	3.18
EU 27 20 cm	20	48	3.77	20.32	18	0.97	2.67	35	1.16	2.82
EU 27 30 cm	30	47	1.99	7.06	12	1.90	5.94	35	1.81	5.64
EU 27 40 cm	40	48	1.82	5.46	11	0.10	1.18	38	1.77	6.94
EU 27 50 cm	50				8	0.72	1.86	47	0.58	2.51
EU 27 60 cm	60	48	1.35	4.48	11	1.07	3.13	39	1.13	4.29
EU 27 70 cm	70				20	1.49	5.14			
EU 27 80 cm	80				18	0.24	1.56			
EU 27 90 cm	90	47	0.80	3.04	7	1.10	2.72			
EU 27 100 cm	100				7	0.17	1.24			
EU 27 110 cm	110	39	0.40	2.29						
Archaeological Features										
EU 27 60E cm (F12)	60				14	0.73	2.10	28	1.79	5.06
EU 27 67E cm (F12)	67	48	2.05	6.77	26	1.86	6.02	31	1.03	3.19
EU 27 76 cm (F12)	76	45	0.38	2.54	7	0.11	1.05	45	1.78	5.75
EU 28 41W cm	41				12	2.01	6.11			
EU 28 68W cm	68				19	0.84	3.42			
EU 29 46W cm (F13)	46				7	0.29	1.20			

5.3 Dosimetry

5.3.1 NAA/DNC Dose Rates

The concentrations of the major radionuclides determined by neutron activation analysis (NAA) and delayed neutron counting (DNC) are given in Table 7, and their changes with depth displayed in Figure 14. Concentrations of ^{238}U and ^{232}Th show a decreasing trend with depth in the sedimentary profile. K concentrations show a sharp increase between -30 to -70 cm depths below the surface, after which concentrations decrease with depth. External dose rates in these samples are largely dominated by the cosmic dose rate.

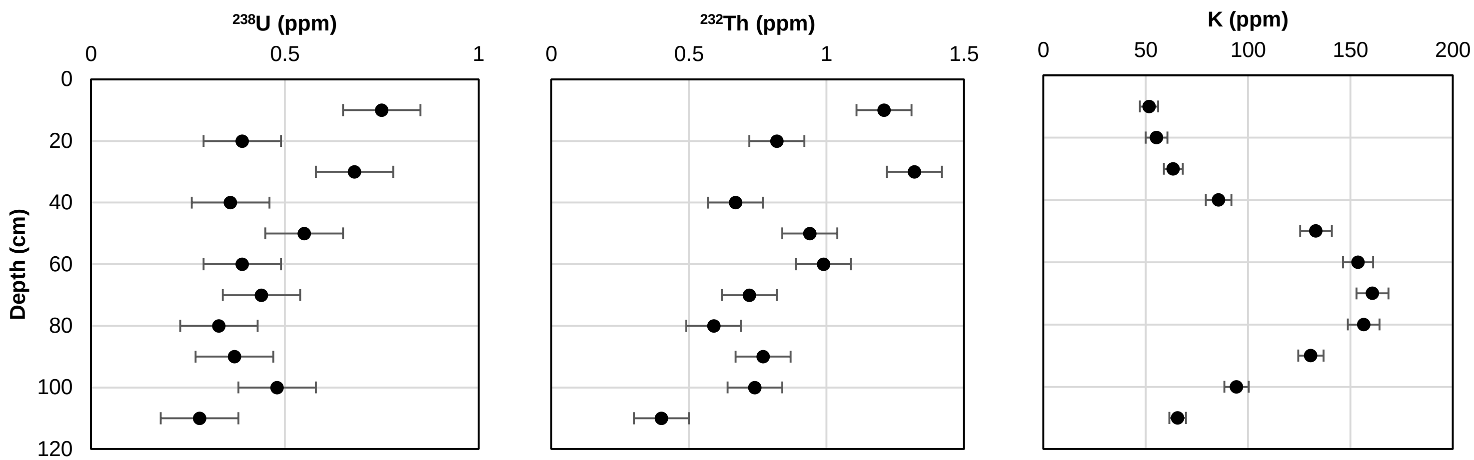

Figure 14 Radionuclide concentrations determined by neutron activation analysis (NAA) and delayed neutron counting (DNC).

Table 7 Dose rates determined using neutron activation analysis (NAA) and delayed neutron counting (DNC) for ^{238}U, ^{232}Th and K

Sample (Feature)	Depth (cm)	^{238}U (ppm)[1]	^{232}Th (ppm)[1]	K (%)[1]	Moisture Content (%)[2]	Cosmic Dose Rate (µGy/a)[3]	External Beta Dose Rate (µGy/a)[4]	Gamma Dose Rate (µGy/a)[4]	Total Dose Rate (µGy/a)[5]
Stratigraphic Section									
EU 27 10 cm	10	0.75 ± 0.1	1.21 ± 0.08	0.00517 ± 0.000445	1.9	271 ± 27	122.8 ± 12.4	139.3 ± 11.5	543.4 ± 17.1
EU 27 20 cm	20	0.39 ± 0.1	0.82 ± 0.03	0.00553 ± 0.000533	1.6	252 ± 25	70.3 ± 12.3	81.7 ± 11.0	414.3 ± 16.7
EU 27 30 cm	30	0.68 ± 0.1	1.32 ± 0.08	0.00635 ± 0.000458	1.2	236 ± 24	118.2 ± 12.5	137.7 ± 11.6	502.2 ± 17.2
EU 27 40 cm	40	0.36 ± 0.1	0.67 ± 0.03	0.00856 ± 0.000621	0.6	223 ± 22	66.2 ± 12.5	72.0 ± 11.1	371.5 ± 16.9
EU 27 50 cm	50	0.55 ± 0.1	0.94 ± 0.04	0.01332 ± 0.000771	6.2	217 ± 22	94.2 ± 11.8	101.0 ± 10.7	422.5 ± 16.1
EU 27 60 cm	60	0.39 ± 0.1	0.99 ± 0.04	0.01537 ± 0.000735	0.5	211 ± 21	82.1 ± 12.5	90.9 ± 11.2	394.3 ± 17.0
EU 27 70 cm	70	0.44 ± 0.1	0.72 ± 0.03	0.01608 ± 0.000778	1.7	205 ± 21	82.0 ± 12.3	82.7 ± 11.0	380.0 ± 16.7
EU 27 80 cm	80	0.33 ± 0.1	0.59 ± 0.03	0.01565 ± 0.000767	0.8	200 ± 20	65.8 ± 12.5	65.0 ± 11.1	341.1 ± 16.9
EU 27 90cm	90	0.37 ± 0.1	0.77 ± 0.05	0.013071± 0.000612	1.6	196 ± 20	72.3 ± 12.4	77.3 ± 11.2	355.9 ± 16.9
EU 27 100 cm	100	0.48 ± 0.1	0.74 ± 0.03	0.00944 ± 0.000590	1.3	194 ± 20	82.8 ± 12.4	88.2 ± 11.1	375.3 ± 16.8
EU 27 110 cm	110	0.28 ± 0.1	0.40 ± 0.03	0.00656 ± 0.000408	1.1	192 ± 19	48.4 ± 12.4	50.0 ± 11.1	300.7 ± 16.8
Archaeological Features									
EU 27 60E cm (F12)	60	0.41 ± 0.1	0.71 ± 0.03	0.00899 ± 0.000661	1.1	211 ± 21	73.3 ± 12.4	79.1 ± 11.1	373.7 ± 16.8
EU 27 67E cm (F12)	67	0.81 ± 0.1	1.78 ± 0.11	0.00762 ± 0.000511	0.7	207 ± 21	146.2 ± 12.7	174.7 ± 12.2	538.2 ± 17.8
EU 27 76 cm (F12)	76	0.79 ± 0.1	1.34 ± 0.08	0.00656 ± 0.000408	2.9	202 ± 20	131.3 ± 12.3	148.5 ± 11.4	491.2 ± 17.0
EU 28 41W cm	41	0.46 ± 0.1	0.87 ± 0.03	0.00703 ± 0.000591	1.1	224 ± 22	81.1 ± 12.4	91.8 ± 11.0	407.3 ± 16.7
EU 28 68W cm	68	0.64 ± 0.1	1.15 ± 0.04	0.01119 ± 0.000760	0.9	206 ± 21	113.4 ± 12.5	125.7 ± 11.2	455.5 ± 16.9
EU 29 46W cm (F13)	46	0.55 ± 0.1	0.81 ± 0.03	0.00732 ± 0.000599	1.3	220 ± 22	91.5 ± 12.4	99.1 ± 11.1	421.0 ± 16.8

1. U, Th, and K values were determined by NAA on sub-samples derived from the OSL samples prior to chemical treatments
2. Water content was calculated as a fraction of dry weight determined from laboratory measurements.

3. Cosmic dose rate value calculated using a linear accumulation model, which assumes half of the present sediment depth and an overburden density of 2 g/cm3
4. These beta and gamma dose rates were calculated based on neutron activation analysis-derived (NAA) U, Th, and K concentrations of each sample accounting for moisture values of the sample. All beta and gamma dose rates are based on an assumption of secular equilibrium in the U and Th decay chains.
5. Includes total internal dose rate of 10.3 ± 2.2 μGy/a

5.3.2 Al_2O_3:C Dose Rates

Results from aluminum oxide dosimetry are outlined in Table 8. External gamma and beta dose rates calculated based on the two methods are further compared in Figure 15 and Figure 16. Only three dose rate values are consistent within error between the two methods for both external beta and gamma dose rates. External beta and gamma dose rates determined from aluminum oxide dosimetry are highly variable throughout the profile, with a relative standard deviation of 114% and 65% respectively. External beta and gamma dose rates determined from NAA and DNC show less variability throughout the profile, with a relative standard deviation of 32% and 37% respectively. Neither external beta nor gamma dose rates calculated using either method show any clear pattern of change with depth in EU 27.

Table 8 Dose rates from Aluminum oxide (Al_2O_3:C) dosimeters

Dosimeter	Corresponding Sample (Feature)	Depth (cm)	Beta + Gamma + Cosmic Dose Rate (μGy/a)[1]	Gamma + Cosmic Dose Rate (μGy/a)[2]	External Beta Dose Rate (μGy/a)	External Gamma Dose Rate (μGy/a)	Cosmic Dose Rate (μGy/a)[3]	Total Dose Rate (μGy/a)[4]
Stratigraphic Section								
HH13	EU 27 10 cm	10	383 ± 50	335 ± 51	41.6 ± 71	99 ± 56	271 ± 27	421.9 ± 90.4
HH14	EU 27 20 cm	20	402 ± 50	354 ± 54	41.6 ± 74	146 ± 57	252 ± 25	449.9 ± 93.4
HH15	EU 27 30 cm	30	657 ± 62	447 ± 67	183.2 ± 91	250 ± 69	236 ± 24	679.5 ± 114.2
HH16	EU 27 40 cm	40	453 ± 53	313 ± 75	104.2 ± 73	145 ± 54	223 ± 22	482.5 ± 90.8
HH17	EU 27 50 cm	50	337 ± 48	494 ± 73	0 ± 88 †	313 ± 75	217 ± 22	540.3 ± 115.6
HH18	EU 27 60 cm	60	688 ± 63	213 ± 35	413.3 ± 72	35 ± 39	211 ± 21	669.6 ± 81.9
HH19	EU 27 70 cm	70	501 ± 54	203 ± 34	258.7 ± 64	26 ± 38	205 ± 21	500.0 ± 74.4
HH20	EU 27 80 cm	80	462 ± 53	357 ± 54	91.1 ± 76	181 ± 60	200 ± 20	482.5 ± 96.8
HH21	EU 27 90cm	90	618 ± 60	220 ± 36	345.5 ± 70	49 ± 39	196 ± 20	600.9 ± 80.1
HH22	EU 27 100 cm	100	245 ± 46	298 ± 46	0 ± 65 †	129 ± 49	194 ± 20	333.3 ± 81.4
Archaeological Features								
HH24	EU 27 76 cm (F12)	76	367 ± 49	378 ± 57	0 ± 75 †	189 ± 60	202 ± 20	401.3 ± 96.0
HH25	EU 27 60E cm (F12)	60	363 ± 49	249 ± 40	98.9 ± 63	52 ± 44	211 ± 21	372.3 ± 76.8
HH26	EU 27 67E cm (F12)	67	273 ± 46	290 ± 45	0 ± 65 †	97 ± 49	207 ± 21	314.3 ± 81.4

† Zero beta dose measurements were assumed to be zero in dose rate calculations but were actually measured as negative values

1. Dose measured from dosimeters not encased in a stainless steel capsule
2. Dose measured from dosimeters encased in stainless steel capsules
3. Cosmic dose rate value calculated using a linear accumulation model, which assumes half of the present sediment depth and an overburden density of 2 g/cm^3 Clarify here that this was calculated, not measured directly, and done only to be able to obtain the gamma dose rate alone.
4. Includes total internal dose rate of 10.3 ± 2.2 μGy/a

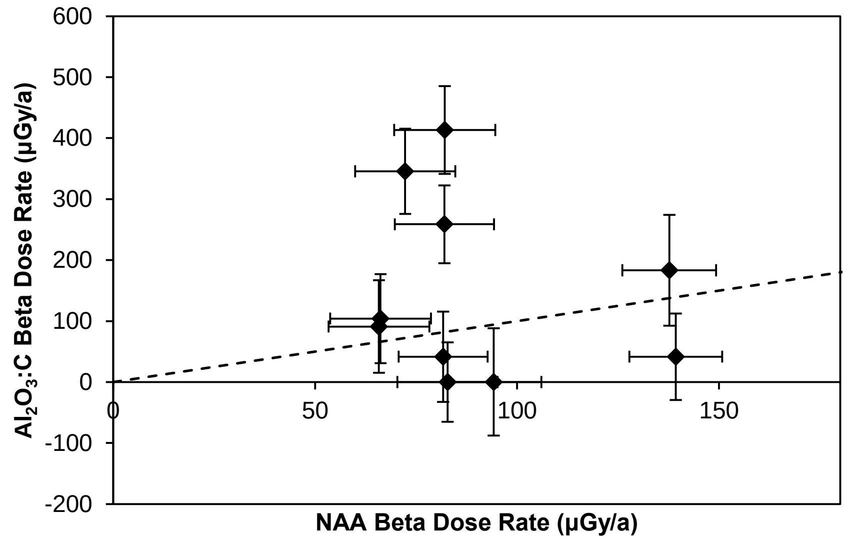

Figure 15 A comparison of the beta dose rate determined by aluminum oxide dosimetry and the beta dose rate determined by neutron activation analysis and delayed neutron counting. The dashed line represents a 1:1 relationship between the two variables.

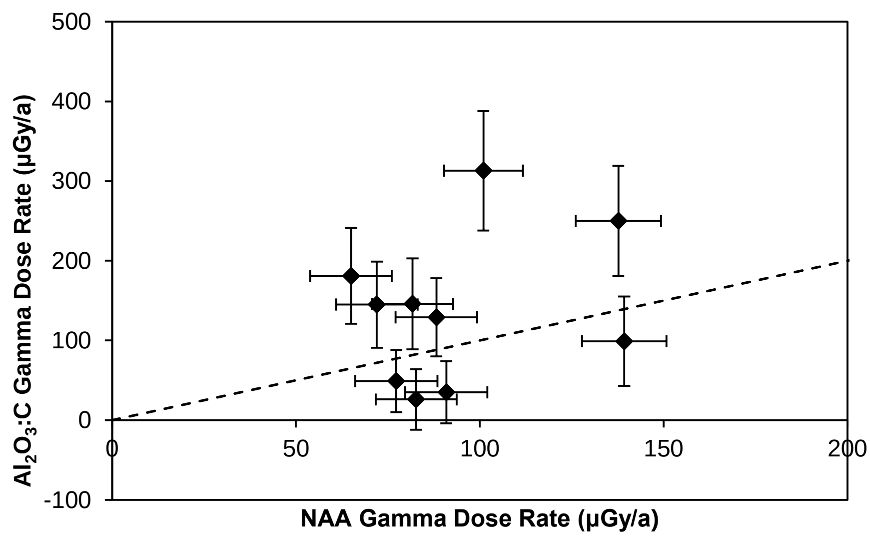

Figure 16 A comparison of the gamma dose rate determined by aluminum oxide dosimetry and the gamma dose rate determined by neutron activation analysis and delayed neutron counting. The dashed line represents a 1:1 relationship between the two variables.

5.4 OSL Ages

Given the presence of multimodal equivalent dose distributions with high overdispersion and a positive skew in our samples, we have attempted to apply the minimum age model (MAM3, Galbraith et al., 1999) and finite mixture model (FMM, Roberts et al., 2000) to isolate the correct burial dose. We have tested the use of the two models at our site by comparing age results with those based on cultural expectation. The minimum age model was able to correctly identify the burial dose for 86% (6/7) of samples within the archaeological horizon, but the finite mixture model was only able to identify the burial dose for 29% (2/7) of samples (Figure 17). This is founded on the assumption that we have correctly estimated the dose rates for these samples (see discussion in the following paragraph), but even when ages are calculated using combinations of other dose rate techniques, results favour the use of the MAM3 over the FMM. Based on this, we have decided to only report ages based on the minimum age model (MAM3).

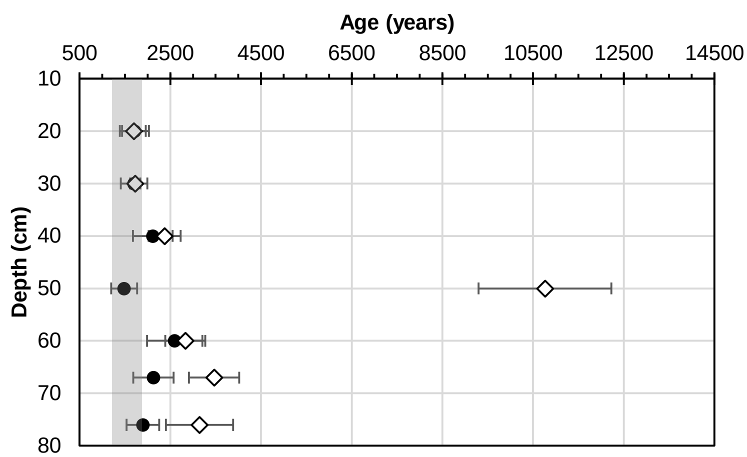

Figure 17 Age results comparing the use of MAM3 and FMM. The shaded region represents the independently established age range of the Swift Creek archaeological culture in northwest Florida. ◇ = FMM, ● MAM3.

In order to determine the most appropriate use of our dosimetry at Harrison Ring, final ages were calculated using results from a combination of techniques and compared over the depth of an archaeological horizon with independent age control (Figure 18):

1) External beta dose rate from NAA/DNC and gamma dose rate from Al_2O_3:C dosimetry
2) External beta and gamma dose rates from Al_2O_3:C dosimetry
3) External beta and gamma dose rates from NAA/DNC

Ages calculated using an external dose rate derived from NAA/DNC (Figure 18c) produced ages that agreed with expectation for 57% (4/7) of samples. Similarly, ages calculated using an external beta and gamma dose rate from Al_2O_3:C dosimetry produced ages that agreed with expectation for 57% (4/7) of samples (Figure 18b). Only those ages calculated using an external beta dose rate from NAA/DNC and gamma dose rate from Al_2O_3:C dosimetry produced ages that agreed with expectation for 86% (6/7) of samples (Figure 18a). Age results beyond this point have been reported using only the latter technique.

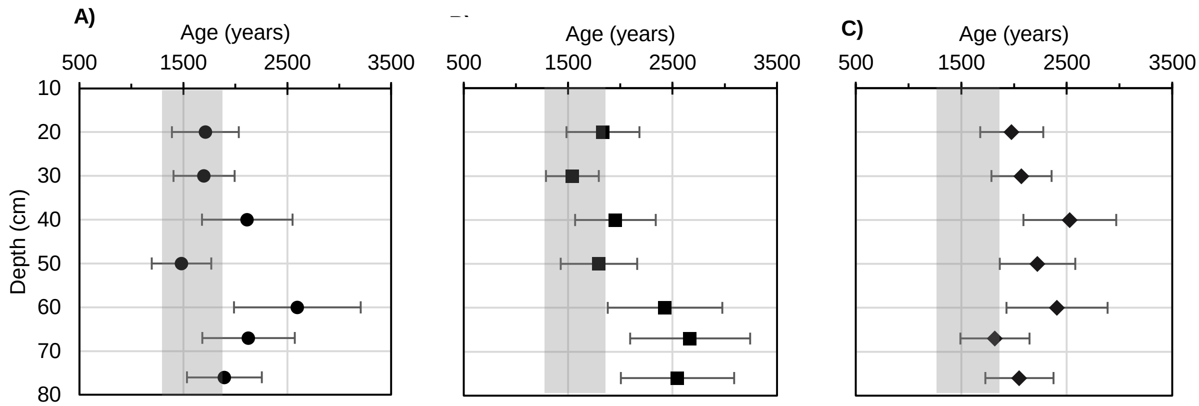

Figure 18 Ages calculated for the archaeological levels at EU 27 using dose rates based on (A) an external beta dose rate from NAA/DNC and gamma dose rate from Al_2O_3:C dosimetry, (B) External beta and gamma dose rates from Al_2O_3:C dosimetry and (C) External beta and gamma dose rates from NAA/DNC. The shaded region represents the independently established age range of the Swift Creek archaeological culture in northwest Florida.

A summary of OSL ages and dose rates used for age calculation is given in Table 9. OSL ages from the vertical profile at EU 27 suggest deposition between ~500 a to ~100 ka (Figure 19), though the 100 ka age may potentially be an overestimate since it was obtained using a 3 mm aliquot. Nevertheless, it probably dates to sometime late in Marine Isotope Stage 5 (> 80 ka). The archaeological horizon, which we interpret to range from -20 to -50 cm depth, has an average single grain MAM3 age of 1751 ± 339 years and average 0.5 mm aliquot MAM3 age of 1613 ± 305 a. Archaeological features in EU 27 exhibit singe grain MAM3 ages that range from 1895 ± 361 a to 2596 ± 610 a. Age results from these same features using 0.5 mm aliquots range from 2735 ± 459 a to 2965 ± 415 a.

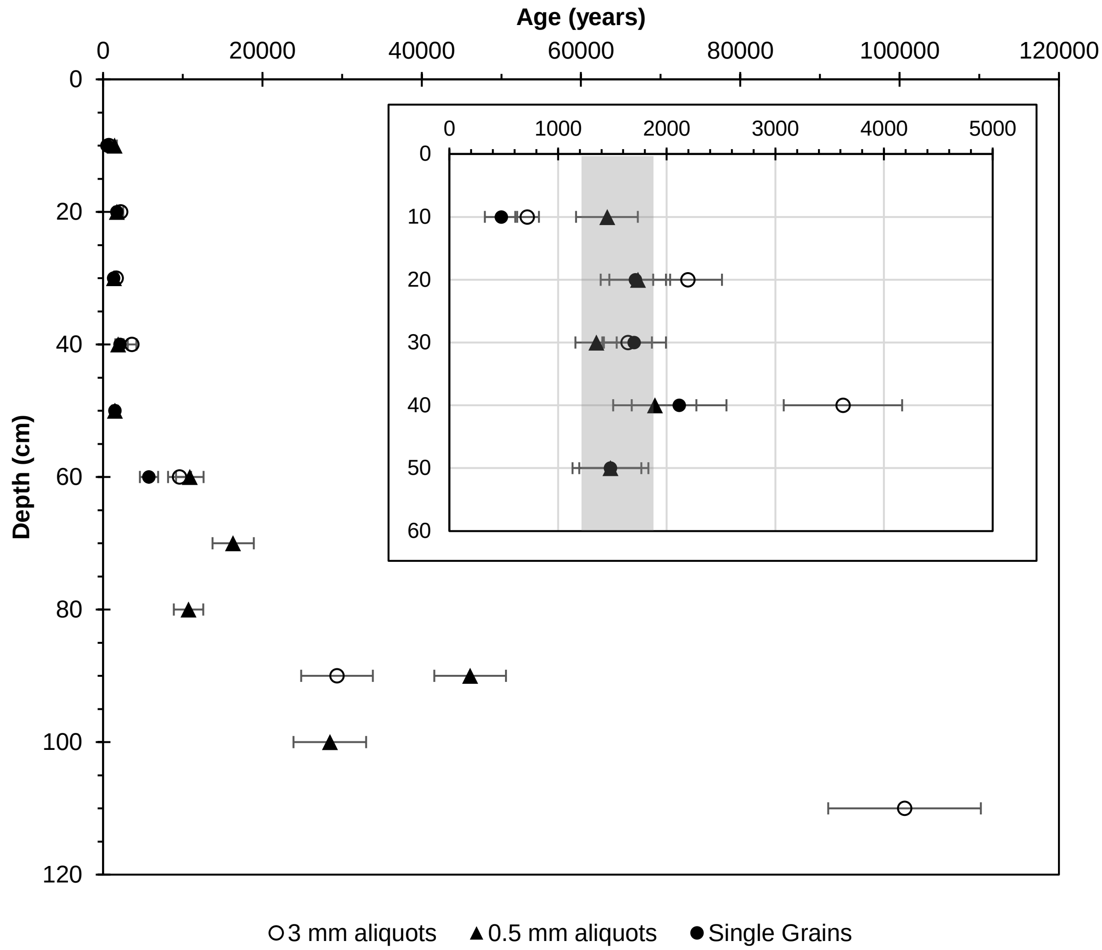

Figure 19 Ages from the stratigraphic section of EU 27. Inset is a close-up view of ages between 0-50 cm depth. The archaeological horizon lies between approximately -20 and -50 cm depth below the surface. The shaded region represents the independently established age range of the Swift Creek archaeological culture in northwest Florida.

Table 9 Summary of dose rates and ages derived from EU 27, EU 28 and EU 29 at Harrison Ring

Sample (Feature)	Depth (cm)	Water Content (%)	Cosmic Dose Rate (µGy/a)	External Beta Dose Rate (µGy/a)	Gamma Dose Rate (µGy/a)	Annual Dose Rate (µGy/a)	3 mm MAM3 age (a)[1]	0.5 mm MAM3 age (a)[1]	Single Grain MAM3 age (a)[1]
Stratigraphic Section									
EU 27 10 cm	10	1.9	271 ± 27	122.8 ± 12.4	99 ± 56	503.1 ± 57.4	715 ± 108	1450 ± 283	476 ± 149
EU 27 20 cm	20	1.6	252 ± 25	70.3 ± 12.3	146 ± 57	478.6 ± 58.3	2193 ± 317	1733 ± 261	1712 ± 321
EU 27 30 cm	30	1.2	236 ± 24	118.2 ± 12.5	250 ± 69	614.6 ± 70.1	1643 ± 221	1350 ± 190	1699 ± 293
EU 27 40 cm	40	0.6	223 ± 22	66.2 ± 12.5	145 ± 54	444.5 ± 55.4	3621 ± 545	1889 ± 383	2114 ± 436
EU 27 50 cm	50	6.2	217 ± 22	94.2 ± 11.8	313 ± 75	634.5 ± 75.9		1481 ± 349	1481 ± 286
Average for archaeological horizons (20 cm – 50 cm)								**1613 ± 305**	**1751 ± 339**
EU 27 60 cm	60	0.5	211 ± 21	82.1 ± 12.5	35 ± 39	338.4 ± 41	9600 ± 1461	10870 ± 1738	5760 ± 1129
EU 27 70 cm	70	1.7	205 ± 21	82.0 ± 12.3	26 ± 38	323.3 ± 40.0		16328 ± 2597	
EU 27 80 cm	80	0.8	200 ± 20	65.8 ± 12.5	181 ± 60	457.1 ± 61.3		10717 ± 1859	
EU 27 90 cm	90	1.6	196 ± 20	72.3 ± 12.4	49 ± 39	327.6 ± 41.0	29359 ± 4497	46084 ± 7336	
EU 27 100 cm	100	1.3	194 ± 20	82.8 ± 12.4	129 ± 49	416.1 ± 50.6		28467 ± 4555	
EU 27 110 cm	110	1.1	192 ± 19	48.4 ± 12.4	50 ± 11.1	300.7 ± 16.8	100629 ± 9570		
Archaeological Features									
EU 27 60E cm (F12)	60	1.1	211 ± 21	73.3 ± 12.4	52 ± 44	346.6 ± 45.7		2798 ± 513	2596 ± 610
EU 27 67E cm (F12)	67	0.7	207 ± 21	146.2 ± 12.7	97 ± 49	460.5 ± 50.6	3321 ± 454	2735 ± 459	2127 ± 444
EU 27 76 cm (F12)	76	2.9	202 ± 20	131.3 ± 12.3	189 ± 60	532.6 ± 61.3	2928 ± 402	2965 ± 415	1895 ± 361
EU 28 41W cm	41	1.6	224 ± 22	81.1 ± 12.4	91.8 ± 11	407.2 ± 16.7			
EU 28 68W cm	68	0.9	206 ± 21	113.4 ± 12.5	125.7 ± 11.2	455.4 ± 16.9		2041 ± 269	
EU 29 46W cm (F13)	46	1.3	220 ± 22	91.5 ± 12.4	99.1 ± 11.1	420.9 ± 16.8		2588 ± 433	

1. Minimum age model (MAM3) D_Es calculated using a σb value of 0 for 3mm aliquots, 0.08 for 0.5 mm aliquots and 0.15 for single grains.

CHAPTER 6: DISCUSSION

Luminescence Characteristics

We have reported ages at Harrison Ring based primarily on OSL measurements of quartz on single grains and 0.5 mm aliquots (~15 grains). Although single grain measurements were only performed on samples within archaeological contexts, with the exception of -10 cm and -60 cm samples in the stratigraphic section, paired measurements on 0.5 mm aliquots (approximately 15 grains per aliquot) generally seemed to recover a statistically comparable result in the stratigraphic profile. This provides confidence in its utility as a replacement for single grain measurements at Harrison Ring. This is also supported by the light sum curves that we report for the stratigraphic section which suggest that the total light sums for these samples are dominated by the signal from approximately 1 grain. Conversely, measurements taken on 0.5 mm aliquots from samples in archaeological features generally do not show agreement with single grain measurements. These samples also displayed light sum curves with a more even distribution of light from their grain populations compared to those samples taken from the stratigraphic section, suggesting that measurements on 0.5 mm aliquots had signals dominated by at least 2 grains. We also observed that samples taken from archaeological features displayed a greater degree of thermally transferred charge at preheat temperatures above 200 °C when compared to those samples taken from the stratigraphic section. Taken together, this suggests that the quartz in these two types of deposits have very different luminescence characteristics. There are two possibilities that could explain these differing characteristics: 1) the quartz grains inside the archaeological features were sourced from different parent material or 2) the quartz grains inside the features experienced a different post-burial history. It is not currently clear which of these may have been the case, but the implication of this is that while multi-grain 0.5 mm aliquots can be reliably used in the stratigraphic profile, they may be problematic for use in the archaeological features.

Equivalent dose distributions and sources of scatter

The sediments at Harrison Ring show a high degree of D_E overdispersion above what has been measured from dose-recovery tests, and also display a positive skew in their D_E distributions throughout the sedimentary profile. These characteristics suggest an external source of scatter that is unrelated to variability in intrinsic luminescence characteristics. Several external sources of equivalent dose scatter been described in the literature, including incomplete bleaching (e.g. Duller, 1994; Olley et al., 1998), variations in microdosimetry (e.g. Murray and Roberts, 1997; Vandenberghe et al., 2003), and post-depositional mixing (e.g. Bateman et al., 2003, 2007). For samples that exhibit a high degree of scatter, it is often most appropriate to use the minimum age model (MAM3) or finite mixture model (FMM) to isolate the meaningful grain populations from the equivalent dose distributions. The minimum age model (MAM3) is used to isolate the youngest grain population and the finite mixture model (FMM) to identify the most prevalent age component. At Harrison Ring, we find the minimum age model to most accurately recover a paleodose when we compare results in locations with independent age control. The FMM was able to recover an accurate equivalent dose for only 29% (2/7) of samples, and otherwise significantly overestimated it.

The sedimentary environment at Harrison Ring, is largely dominated by the cosmic ray component, which makes up ~30-65% of the total dose rate in our samples. This is a common feature in many Florida sites that have been studied with OSL (eg. Rink and Lopez, 2010; Lopez, 2007; Thompson et al., 2007). It has been shown in the literature that quartz rich sands can often show a significant degree of beta dose rate heterogeneity because they can be influenced by small quantities of beta emitters (eg. feldspars, heavy minerals) in the sedimentary matrix (Mayya et al., 2006; Chauhan and Singhvi, 2011). Our results from Al_2O_3:C dosimetry suggest a significant amount of beta dose-rate heterogeneity in the sediments at Harrison Ring. This beta dose-rate variability was not captured by analyses using neutron activation analysis and delayed neutron counting, which measure an average dose-rate over a volume of approximately 65 g of mixed sediment that is then sampled to 1 g. This averaging of the dose rate using NAA/DNC masks the high degree of variability that exists at smaller scales and can only be captured using in-situ Al_2O_3:C beta dosimetry.

The Al_2O_3:C dosimetric measurements that we present are the first to ever be used in a dating context. In a complex dosimetric environment like that seen at Harrison Ring, we find the combination of NAA/DNC and Al_2O_3:C techniques for determining a dose rate to be advantageous. By testing the combination of techniques in an area with independent age control, we have found that the most suitable way of determining a dose rate at Harrison Ring is by using beta dosimetry from NAA/DNC which represents a large volumetric average (~65 grams of sediment), and gamma dosimetry from in-situ Al_2O_3:C dosimeters, which average the dose over a 30 cm radius volume. By using beta and gamma dosimetry from NAA/DNC exclusively, we find ages to be largely overestimated. Likewise, we find that using external beta and gamma dosimetry from in-situ Al_2O_3:C dosimetry often overestimates ages for these archaeological samples. By using gamma dosimetry from Al_2O_3:C dosimeters, we should be able to obtain a more accurate dose rate that covers the full 30 cm range of gamma rays. However, for capturing the appropriate beta dose rate in sediments with a high degree of heterogeneity, it should theoretically be more appropriate to use measurements based on a volumetric average, and not from small-scale Al_2O_3:C dosimetry, which can be heavily influenced by radioactive hot or cool spots within only 2 mm of the dosimeter wrapped in electrical tape.

Bioturbation has also been suggested as a cause for equivalent dose scatter and erroneous age determinations in a number of archaeological studies (eg. Balek, 2002; Bateman et al., 2007; Forrest et al., 2003; Rink et al., 2012a, b; Thulman, 2012; Wilder et al., 2007). In Florida, discordance between radiocarbon ages and OSL ages in archaeological sites has been a consistent issue that has often been attributed to bioturbation (Wilder et al., 2007; Rink et al., 2012a, b). As a result of these prevalent issues, a small body of literature has begun to emerge on the fundamentals of OSL in bioturbated environments, pioneered by Bateman and colleagues. Bateman et al. (2003) have examined the influence of pedoturbation on OSL equivalent dose and have outlined a number of hypothetical effects of bioturbation on equivalent dose distributions. Bateman et al. (2007) reported results for a number of different sites and concluded that high overdispersion, equivalent dose skewness, trends in zero dose grains appeared good indicators of post-depositional disturbance.

Incomplete bleaching is another potential source of equivalent dose scatter, but is mainly associated with fluvially deposited sediments because exposure to sunlight can be reduced by the depth and turbidity of the water column (Olley et al., 1998). The sediments at Harrison Ring are the result of aeolian deposition and in the archaeological features, possibly some anthropogenic processes, but we have no sedimentary or geomorphological evidence to believe that fluvial processes have been active at our study site. We therefore believe that the most likely causes of equivalent dose scatter at this site are beta-microdosimetry and/or post-depositional mixing.

OSL age results

We report a history of sediment accumulation at Harrison Ring that spans from approximately 100,000 years for the deepest sample to 500 years before present for the shallowest sample. Excluding the measurements of 0.5 mm aliquots of 80 cm and 100 cm samples at EU 27, all samples produce internally consistent results that preserve stratigraphic order. At -110 cm below depth we report an OSL age of ~100,000 +/- 10,000 a, which dates to a shoreline at Harrison Ring that is consistent with deposition during the last interglacial (MIS 5). Burdette et al. (2012) found ages further southeast on the Gulf coast at a similar elevation above sea level that agree with the age that we report. After a period of slow aeolian accumulation, humans, namely the Swift Creek peoples, occupied the landscape at Harrison Ring. We report a mean MAM3 OSL age for the archaeological horizon between -20 and -50 cm depth in EU 27 to be 1751 ± 339 a for single grain measurements and 1613 ± 305 a for measurements on 0.5 mm aliquots. These OSL age ranges are fully consistent with expectation based on Swift Creek occupation in northwestern Florida, and the radiocarbon dates that were previously collected from the site (see Table 1 and Appendix A, Table 1 for details). Above this archaeological horizon, OSL evidence also suggests that this deposit has accumulated an aeolian sequence up to about 20 cm thick in the last ~1500 years, with an age of as young as 330 years ago at -10 cm. Although the coastal lands that exist seaward of Harrison Ring have not yet been dated, it is probable that they formed in the late Holocene like all the other sand spits and islands in the region (eg. Rink and Lopez, 2010). Dating would be needed in the future to determine whether these frontal peninsulas were in place at the time of Swift Creek occupation at Harrison Ring.

OSL ages determined from samples in archaeological features were often overestimated, even at the single grain level, when compared to radiocarbon age control at the site. At EU 27/28 in Feature 12, two radiocarbon dates were previously obtained from at a depth of 65-70 cm below the surface: a *Busycon sinistum* fragment, which had a calibrated age of 1425-1225 cal BP, and a turkey bone fragment with a calibrated age of 1365-1245 cal BP. These archaeological features have been interpreted as single episodic events, meaning that a pit was dug into underlying soils, and artifacts either fell into or were placed in the pit over a single event (Dengel, 2014 pers. comm.). If this is true, the OSL ages that we have determined from these features should theoretically match with those radiocarbon ages taken from the same features. There are at least two possible reasons why the radiocarbon dates from these features and the OSL ages are not consistent. We are unclear how the pits were filled, and depending on how the pit was filled, the number of zeroed grains recording the burial event could have been proportionately small and difficult to capture using OSL. The possibility also exists that the samples obtained from these features were actually outside of the pit and captured some older sands. The three single grain OSL ages from Feature 12 are all overestimated relative to those two radiocarbon ages, but EU 27 67 cm and EU 27 76 cm still produce ages that are consistent within error with early Swift Creek occupation in northwest Florida. The ages that we calculated from these two samples in Feature 12 are also consistent with the ages we find in the archaeological horizon of the adjacent stratigraphic profile. These two OSL samples correspond to the locations of two artifacts: a worked quartz cobble and a kirk point, both found at 67 cm below the surface.

Theoretically, there are at least two major benefits to employing the use of OSL dating over radiocarbon dating. By using OSL, there is no need to rely on the presence of associated organic material that can be used for dating. Moreover, the ages that are reported using OSL are expressed in calendar years before present, and do not rely on calibration. At Harrison Ring specifically, there are also some concerns about the way in which reservoir corrections for radiocarbon dates on shell have been very recently locally developed and applied. The major problem with the OSL ages that we report are that the errors are very large compared to radiocarbon dates. For single grain measurements, these error terms can range from ~18-23% in our single grain measurements, and ~13-18% in our 3 mm and 0.5 mm multi-grain measurements. The 1σ standard deviation on the mean age for the -20 to -50 cm archaeological levels is 19%. These relatively large errors are not intrinsic to OSL, but to the site characteristics probably dominated by problematic beta dose rate heterogeneity. These error terms are large compared to the radiocarbon ages at the site that have errors less than 5%.

CHAPTER 7: CONCLUSIONS

The project at Harrison Ring began with the expectation that OSL age determination on sediments would provide age constraints on the timing of the Swift Creek occupation at the site. This research presents the very first Swift Creek site dated using OSL. While the large errors on the OSL ages that we measured did not permit for the determination of the onset and ending of occupation at the site, we were able to calculate an average age for the occupation of approximately 1751 ± 339 years ago. This is fully consistent with radiocarbon age control at the site and fits into the accepted cultural chronology of the Swift Creek occupation in northwest Florida. This successful result is particularly meaningful because it highlights the success of using OSL in a low dose rate sedimentary environment which has been affected by beta dose rate heterogeneity and possible post-depositional mixing. The success of these OSL ages is due, in part, to the effective implementation of dosimetric techniques at the site. We find based on our testing of these dosimetric techniques that OSL ages calculated using beta and gamma dose rates from NAA or beta and gamma dose rates from Al_2O_3:C dosimeters alone are largely overestimated relative to age control at the site. At Harrison Ring, the most successful approach in dealing with sediments that express a high degree of beta dose rate heterogeneity is to utilize a combination of dosimetric techniques: in-situ Al_2O_3:C for gamma dose rate determination and volumetric NAA for beta dose rate determination. To summarize, based on the results of this study, we have concluded that:

1) OSL evidence shows that at -110 cm, we find a deposit that is ~ 100,000 years old and is consistent with a deposit produced during the last interglacial, MIS 5.
2) OSL evidence suggests that the sampled sedimentary profile was an accumulating geological sequence after that time, which predates the arrival of humans in North America based on most reckoning of arrival time.
3) OSL evidence supports the idea that humans modified the landscape approximately 1751 ± 339 years ago (based on single grain measurements), which is fully consistent with the timing of early Swift Creek cultures on the Florida Gulf Coast. The age that we report is both consistent with radiocarbon dates taken at Harrison Ring, and those taken at other Swift Creek sites on the Gulf Coast Appendix A, Table 1). After modification by the Swift Creek peoples, sediment continued to accumulate at this site until approximately 400 years ago.
4) Single grain OSL ages from an archaeological feature are overestimated relative to radiocarbon ages from the same feature, but have ages that are consistent within error with early Swift Creek occupation in northwest Florida. These ages correspond to two adjacently located artifacts: a worked quartz cobble and a kirk point, each at -67 cm.
5) OSL equivalent doses show high overdispersion and skewness, likely as a result of beta-microdosimetry and/or bioturbation in the profiles.
6) Al_2O_3:C dosimetry has been used to show that large variability in beta dose rates exist in the sedimentary profile at Harrison Ring.
7) Dosimetry results from Al_2O_3:C and NAA/DNC are widely different, but generally we find that the best agreement with independent age control exists when calculating ages using a beta dose rate from NAA/DNC and gamma dose rate from Al_2O_3:C dosimetry. This suggests that when working in sediments with low dose rates and heterogeneous beta dose rates like those seen on the Gulf Coast, Al_2O_3:C dosimetry may not be appropriate for determining the beta dose rate used for age calculation.

8) OSL measurements made on small (0.5 mm) aliquots with ~15 grains yield MAM3 age results that are statistically indistinguishable from single grain measurements in the stratigraphic profile, and could have therefore been used for age determination at this site, though the latter aliquot technique would have yielded a mean age about 150 years younger than using the single grains. In archaeological features, 0.5 mm aliquots generally yield age overestimates when compared to single grains. This is consistent with the results of cumulative light-sum curves that show different characteristics for the two types of deposits studied. In samples taken from archaeological features, we find that there may be at least 2 grains contributing to the OSL signal on a 0.5 mm aliquot with ~15 grains.

REFERENCES

Adamiec, G., & Aitken, M. (1998). Dose-rate conversion factors: update. *Ancient TL*, *16*(2), 37–50.

Antoine, P., Rousseau, D.D., Zöller, A., Lang, L., Munaut, A.V., Hattè, C., Fontugne, M., 2001. High-resolution record of the last Interglacial-glacial cycle in the Nussloch loess-palaeosol sequences, Upper Rhine Area. Germany. *Quaternary International, 76/77*, 211–229.

Ashley, K. H.,Wallis, N. (2006). Northeastern Florida Swift Creek: an overview and future research directions. *The Florida Anthropologist, 59*, 5-18.

Balek, C. (2002). Buried artifacts in stable upland sites and the role of bioturbation: a review. *Geoarchaeology*, *17*, 41-51

Bateman, M.D., Boulter, C.H., Carr A.S., Frederick, C.D., Peter, D., Wilder, M. (2007) Preserving the palaeoenvironmental record in drylands: bioturbation and its significance for luminescence-derived chronologies. *Sedimentary Geology*, *195*, 5–19.

Bateman, M.D., Frederick, C.D., Jaiswal, M.K. & Singhvi, A.K. (2003). Investigations into the potential effects of pedoturbation on luminescence dating. *Quaternary Science Reviews, 22*, 1169–1176.

Bense, J.A. (1989). Pensacola archaeological survey and summary of archaeology in the Pensacola area of west Florida to 1988. The Pensacola Archaeological Society, Publication 2.

Bense, J.A. (1998). Santa Rosa – Swift Creek in Northwestern Florida. In A World Engraved: Archaeology of the Swift Creek Culture, edited by M. Williams and D.T. Elliot, pp. 247-273. University of Alabama Press, Tuscaloosa.

Bøtter-Jensen, L., McKeever, S.W.S, Wintle, A.G. (2003). Optically Stimulated Luminescence Dosimetry. Elsevier, Amsterdam.

Braun, E.L. (1950). Deciduous forests of eastern North America. The Free Press, MacMillan, New York.

Burdette, K. E., Rink, W. J., López, G. I., Mallinson, D. J., Parham, P. R., & Reinhardt, E. G. (2012). Geological investigation and optical dating of Quaternary siliciclastic sediments near Apalachicola, North-west Florida, USA. *Sedimentology*, *59*(6), 1836–1849.

Chauhan, N, Singhvi, A.K. (2011) Distribution of SAR paleodoses due to spatial heterogeneity of natural beta dose. *Geochronometria,* 38, 190–198

Duffee, E.M., Baldwin, R.A., Lewis, D.L., Warmack, W.B. (1984). Soil survey of Bay County, Florida. U.S. Department of Agriculture, Soil Conservation Service. Washington, DC.

Duller, G.A.T. (1994). Luminescence dating of poorly bleached sediments from Scotland. *Quaternary Geochronology, 13*, 521–524.

Duller, G.A.T., Bøtter-Jensen, L., Murray, A.S. (2000). Optical dating of single sand-sized grains of quartz: sources of variability. *Radiation Measurements, 32,* 453-457.

Duller, G.A.T. (2008). Luminescence Dating: guidelines on using luminescence dating in

archaeology. Swindon: English Heritage.
Forrest, B., Rink, W.J., Bicho, N., Ferring, C.R. (2003). OSL ages and possible bioturbation signals at the Upper Paleolithic site of Lagoa do Bordoal, Algarve, Portugal. *Quaternary Science Reviews, 22*, 1279–1285.
Galbraith, R.F.,Roberts, R.G., Laslett, G.M.,Yoshida, H., Olley, J.M. (1999). Optical dating of single and multiple grains of quartz from jinmium rock shelter, northern Australia, Part 1: experimental design and statistical models. *Archaeometry, 41*, 339-364.
Galbraith, R. F., Roberts, R. G., & Yoshida, H. (2005). Error variation in OSL palaeodose estimates from single aliquots of quartz: a factorial experiment. *Radiation Measurements*, *39*(3), 289–307.
Guérin, G., Mercier, N., Adamiec, G. (1998). Dose-Rate Conversion Factors: Update. *Ancient TL*, *29*(1): 5-8.
Kalchgruber, R., Fuchs, M., Murray, A.S., Wagner, G.A., 2003. Evaluating dose-rate distributions in natural sediments using a-Al2O3:C grains. *Radiation Measurements,* 37, 293-297.
Kalchgruber, R., & Wagner, G. A. (2006). Separate assessment of natural beta and gamma dose-rates with TL from a-Al2O3: C single-crystal chips. *Radiation Measurements*, *41*, 154–162.
Kirkland, S.D. (2003). Human Prehistory at the Sadlers Landing Site, Camden County, Georgia. *Early Georgia, 31*, 107-192
Lopez, G. (2007). Optical dating of barrier islands in the Gulf of Mexico. Ancient TL – published theses. http://www.aber.ac.uk/ancient-tl/.
MacNeil, F.S. (1950). Pleistocene shore lines in Florida and Georgia. U.S. Geological Survey Professional Papers 221-F, pp. 95-107.
Mayya, Y.S., Morthekai, P., Murari, M.K., Singhvi, A.K. (2006). Towards quantifying beta microdosimetric effects in single-grain quartz dose distribution. *Radiation Measurements, 41,* 1032-1039.
Mejdahl, V. (1979). Thermoluminescence dating: beta-dose attenuation in quartz grains. *Archaeometry*, *21*, 61–72.
Mercier, N., Gaugez, C. (2012). ANATOL v. 2.0.52 [computer software]. LSCE – Domaine du CNRS, Gif-sur-Yvette, France.
Milanich, J. (1994). Archaeology of Precolumbian Florida. Gainesville: University Press of Florida.
Moore, C.B. (1902). Certain Aboriginal Remains of the Northwest Florida Coasts, Part II. *Journal of the Academy of Natural Sciences of Philadelphia, 12,* 128-358.
Moore, C.B. (1918). The *Northwestern Florida Coast Revisited. Journal of the Academy of Natural Sciences of Philadelphia, 16,* 514-580.
Murray, A.S., Roberts, R.G. (1997). Determining the burial time of single grains of quartz using optically stimulated luminescence. *Earth Science Planetary Letters*, *152*, 163–180.
Murray, A.S, Wintle, A.G. (2000). Luminescence dating of quartz using an improved single-aliquot regenerative-dose protocol. *Radiation Measurements, 32*, 57-73.
Murray, A.S., Wintle, A.G. (2003). The single aliquot regenerative dose protocol:

potential improvements in reliability. *Radiation Measurements, 37,* 377-381.

Musgrove, R.H., Foster, J.B., Toler, L.G. (1965). Water resources of the Ecofina Creek Basin in northwestern Florida. Florida Division of Geology, Information Circular 57.

NOAA. (1997). Coastal Hazardous Waste Site Review / Tyndall Airforce Base. pp. 82.

Olley, J.M., Caitcheon, G.G., Murray, A.S. (1998). The distribution of apparent dose as determined by optically stimulated luminescence in small aliquots of fluvial quartz: implications for dating young sediments. *Quaternary Science Reviews, 17,* 1033–1040.

Penton, D. T. (1974). Early Swift Creek phase in north Florida: Internal expressions and external connections. Paper presented at the 39th annual meeting of the society for American archaeology, Washington.

Phelps, D. D. (1969). Swift Creek and Santa Rosa in Northwest Florida. Institute of Archaeology and Anthropology, University of South Carolina Notebook. 1, 14-24.

Polf, J. C., McKeever, S. W. S., Akselrod, M. S., Holmstrom, S. (2002) A real-time, fibre optic dosimetry system using Al_2O_3 fibre. *Radiation Protection Dosimetry*, 100, 301–304.

Prescott, J. R., Hutton, J. T. (1988). Cosmic Ray and Gamma Ray Dosimetry for TL and ESR. *Nuclear Tracks and Radiation Measurements*, *14*(1/2), 223–227.

Puri, H.S., Vernon, R.O. (1964). Summary of the geology of Florida and a guidebook to the classic exposures (revised). Florida Geological Survey Special Publication no.5. Tallahassee.

Rhodes, E. J. (2011). Optically Stimulated Luminescence Dating of Sediments over the Past 200,000 Years. *Annual Review of Earth and Planetary Sciences*, *39*(1), 461–488.

Rink, W. J., Dunbar, J. S., Burdette, K. E. (2012a). The Wakulla Springs lodge site (8Wa329): 2008 excavations and new OSL dating evidence. *Florida Anthropological Society*, *65*(1-2), 5–23.

Rink, W. J., Dunbar, J. S., Doran, G. H., Frederick, C., Gregory, B. (2012b). Geoarchaeological investigations and OSL dating evidence in an archaic and paleoindian context at the Helen Blazes Site (8Br27), Brevard County, Florida. *Florida Anthropological Society*, *65*(1-2), 87–107.

Rink, W. J., & López, G. I. (2010). OSL-based lateral progradation and aeolian sediment accumulation rates for the Apalachicola Barrier Island Complex, North Gulf of Mexico, Florida. *Geomorphology*, *123*(3-4), 330–342.

Rink, W.J., Odom, A.L. (1991). Natural alpha recoil particle radiation and ionizing radiation sensitivities in quartz detected with EPR: implication for geochronometry. *Nuclear Tracks and Radiation Measurements, 18*, 163–173.

Roberts, R.G., Galbraith, R.F., Yoshida, H., Laslett, G.M., Olley, J.M. (2000). Distinguishing dose populations in sediment mixtures: a test of single-grain optical procedures using mixtures of laboratory-dosed quartz. *Radiation Measurements, 32*, 459–465.

Russo, M., Hadden, C.S., Dengel, C. (2009). Archaeological investigations of mounds and ring middens at Hare Hammock – Tyndall Air Force Base. Southeast Archaeological Center National Park Service.

Russo, M., Dengel, C., Shanks, J., McFeaters, A. (2014). Archaeological determinations of boundaries and cultural affiliations at the Hare Hammock 8By31 site. Southeast Archaeological Center National Park Service.

Sears, W.H. (1962). Hopewellian affiliations of certain sites on the Gulf Coast of Florida. *Amarican Antiquity, 28*(1), 5-18.

Schmidt,W. & Wiggs-Clark, M. (1980). Geology of Bay County, Florida. Florida Bureau of Geology Bulletin no. 57. Tallahassee, FL.

Shanks, J., Byrd, J.C. (2012). Shell game: the marine reservoir effect and the chronology of a Woodland mound and ring complex on the northwest Florida coast. Paper presented at the annual meeting of the southeastern archaeological conference, Baton Rouge.

Stephenson, K., Bense, A.J., Snow, F. (2002). Aspects of Deptford and Swift Creek of the South Atlantic, in The Woodland Southeast, edited by Anderson and Mainfort, pp. 318-340. University of Alabama Press, Tuscaloosa

Thomas, P., Campbell, J. (1993). Eglin Air Force Base Historic Preservation Plan. Technical Synthesis of Cultural Resource Investigations at Eglin, Santa Rosa, Okaloosa, and Walton Counties Florida. Report of Investigations 192. New World Research, Inc., Fort Walton Beach, Florida.

Thomas, P.M., Meyer, J., Adams, W. (1996). Cultural resources survey: Camp Helen, Bay County, Florida. Prentice Thomas and Associates, Inc. Report of Investigations Number 305. Fort Walton Beach, Florida.

Thompson, J., Jack Rink, W., & López, G. I. (2007). Optically stimulated luminescence age of the Old Cedar midden, St. Joseph Peninsula State Park, Florida. *Quaternary Geochronology*, *2*(1-4), 350–355.

Thulman, D. K. (2012). Bioturbation and the Wakulla Springs lodge site artifact distributions. *The Florida Anthropologist*, *65*(1-2), 25–34.

Vandenberghe, D., Hossain, S.M., De Corte, F., Van den haute, P., 2003. Investigations on the origin of the equivalent dose distribution in a Dutch cover sand. *Radiation Measurements,* 37, 433-439.

Wilder, M., Frederick, C.D., Bateman, M.D., Peter, D.E. (2007). Geoarchaeological investigations in the flats of the Osceola Plain, Highlands and Polk Counties, Florida. *The Florida Anthropologist, 60*, 97-116.

Willey, G.R. (1949). Archaeology of the Florida Gulf Coast. Smithsonian Miscellaneous Collections 115. Washington, D.C. Reprinted by University Press of Florida, Gainesville, 1998.

Williams, J. M., Elliott, D.T. (1998). Swift Creek Research: History and Observations. In A World Engraved: Archaeology of the Swift Creek Culture. Tuscaloosa: University of Alabama Press.

APPENDIX A

Table 1 Radiocarbon ages from Swift Creek sites on the Florida Gulf Coast excluding those from Harrison Ring (Adapted from Stephenson et al., 2002). Radiocarbon dates taken from Harrison Ring can be found in Table 2 in the main text.

Site No.	**Site Name**	**Calibrated radiocarbon age (cal BP) (max – min range) (1 sigma)**	**Reference**
8SR8	Third Gulf Breeze	A.D. 624 – 770	Phelps (1969)
8WL36	Horseshoe Bayou	A.D. 555 – 668	Thomas and Campbell (1993)
8SR986	Bernath	A.D. 642 – 689	Bense (1998)
8WL36	Horseshoe Bayou	A.D. 611 – 697	Thomas and Campbell (1993)
8SR986	Bernath	A.D. 544 – 647	Bense (1998)
8LI172	Otis Hare	A.D. 475 – 653	Nancy White, pers. comm. (2001)
8SR8	Third Gulf Breeze	A.D. 441 – 653	Phelps (1969)
8LI172	Otis Hare	A.D. 431 – 615	Nancy White, pers. comm. (2001)
8LI172	Otis Hare	A.D. 397 – 598	Nancy White, pers. comm. (2001)
8SR986	Bernath	A.D. 411 – 540	Bense (1998)
8FR4	Tucker	A.D. 73 – 765	Phelps (1966)
8SR986	Bernath	A.D. 343 – 431	White (1992)
8GU38	Overgrown Road	A.D. 343 – 431	White (1992)
8WL58	Old Homestead	A.D. 168 – 353	Thomas et al. (1996)
8WL58	Old Homestead	A.D. 69 – 236	Thomas et al. (1996)